THEF-NIJM 91.02

Strangeness exchange in antiproton-proton scattering*

R.G.E. Timmermans, Th.A. Rijken, and J.J. de Swart
Institute for Theoretical Physics, University of Nijmegen, Nijmegen, the Netherlands

Abstract

A model is presented for the production of antihyperon-hyperon pairs in antiproton-proton scattering in the energy region below 2.0 GeV/c antiproton laboratory momentum accessible at LEAR. An antibaryon-baryon potential is constructed from the Nijmegen soft-core OBE nucleon-nucleon and hyperon-nucleon potential. Using this potential as intermediate- and long-range interaction the multichannel Schrödinger equation is solved with a complex boundary condition at $r = b = 1.2$ fm. The model is applied to the elastic $\overline{p}p \to \overline{p}p$ scattering data, cross sections, and asymmetries at intermediate energies around 1.5 GeV/c antiproton momentum. Next we compare it to the full set of data, cross sections, polarizations, and spin correlations, on the strangeness-exchange reaction $\overline{p}p \to \overline{\Lambda}\Lambda$ which has its threshold at momentum 1435 MeV/c. Excellent results are obtained. Fitting 157 observables at 6 different energies we reach $\chi^2_{\rm min} = 180.6$, corresponding to $\chi^2/{\rm data} = 1.15$. The results demonstrate the dominance of the strangeness-changing tensor force due to the combined exchange of the $K(494)$ and $K^*(892)$ mesons.
The method of calculation is similar to the one employed in the Nijmegen partial-wave analyses of low-energy proton-proton and neutron-proton scattering data. In the same manner we perform a 'model-independent' partial-wave analysis of the reaction $\overline{p}p \to \overline{\Lambda}\Lambda$ close to threshold. The S-matrix elements are presented.

PACS numbers: 13.75.Cs, 11.80.Gw, 21.40.Qq

*Published in Phys. Rev. **D45**(1992), 2288-2307)

I. INTRODUCTION

Recently the data taken in the first runs of the PS185 experiment at the LEAR facility of CERN have been published [1, 2, 3], as earliest results of the ongoing investigation of the antihyperon-hyperon channels below 2.0 GeV/c antiproton laboratory momentum. These new data on the reaction $\overline{p}p \to \overline{\Lambda}\Lambda$ are qualitatively much better than the old bubble-chamber data [4, 5]. The $\overline{Y}Y$ thresholds that LEAR is planned to reach in the immediate future are shown in Table I (the $\overline{\Xi}^0\Xi^0$ and $\overline{\Xi}^-\Xi^-$ channels are not yet within the energy range of LEAR). Experimentally the antihyperon-hyperon final state can be detected clearly because the hyperons decay weakly into a nucleon and a pion. In the case of the $\overline{p}p \to \overline{\Lambda}\Lambda$ reaction all four charged decay products can be detected. In $\overline{p}p \to \overline{\Lambda}\Sigma^0, \overline{\Sigma^0}\Lambda$ the fast electromagnetic decay of Σ^0 into $\Lambda\gamma$ can be experimentally taken into account [6]. In charged $\Sigma^\pm$ production only two out of four decay particles carry charge, but on the other hand the hyperons themselves leave traces. As a consequence in all these reactions the kinematics of the two-body scattering process can be reconstructed completely. Moreover, since these parity non-conserving decays have a large asymmetry with respect to the polarization axis of the hyperons, a complete set of observables including polarizations and spin correlations may be measured without the need for a polarized target or secondary scattering. Referring to these favorable circumstances, these reactions are called 'self-analyzing'. Another nice feature is that the LEAR beam can be tuned to energies close to threshold where only relatively few partial waves contribute.

Theoretically the $\overline{p}p \to \overline{Y}Y$ reactions constitute a unique means for studying strangeness production. This can be done either in a conventional meson-exchange approach where the exchange of at least one strange meson is required, or with constituent-quark models where at least one $\overline{s}s$ pair must be created. In fact hopes have been expressed that with these reactions one can probe the underlying quark structure of the baryons involved. One simple example is the following. In the quark model the spin of the hyperon can be related directly to the spin of its strange quark. For instance, it is easy to see that in the reaction $\overline{p}p \to \overline{\Lambda}\Lambda$ the spin of the $\overline{s}s$ pair is exactly equal to the spin of the $\overline{\Lambda}\Lambda$ pair. Experimentally near threshold the $\overline{\Lambda}\Lambda$ pair is produced almost exclusively in the triplet state. The $\overline{s}s$ pair is thought to be created either with $^3S_1$ or $^3P_0$ quantum numbers, corresponding to $J^{PC} = 1^{--}$ or $J^{PC} = 0^{++}$. The threshold behavior of the cross section is given by $\varepsilon^{\ell+\frac{1}{2}}$. Here $\varepsilon = \sqrt{s} - 2m_\Lambda$ is the kinetic energy and ℓ is the relative orbital angular momentum of the $\overline{\Lambda}\Lambda$ pair (s is the total energy in the center-of-mass system). The argument is often made that from the threshold behavior of the $\overline{p}p \to \overline{\Lambda}\Lambda$ reaction it is possible to determine which is the underlying pair creation model. Thus S-wave behavior should correspond to the $^3S_1$ and P-wave behavior to the $^3P_0$ pair creation model. However, things are not that simple. The argument disregards the Fermi motion of the spectator non-strange quarks. As a result even in the $^3P_0$ pair creation model S-wave behavior of the cross section close to threshold is possible instead of the naively expected P-wave behavior [7].

Before 1980 several Regge-pole models were proposed to explain the bubble-chamber data [5, 8, 9], which were taken mostly at higher energies. The most successful models included the $K^*(892)$ trajectory as the dominant ingredient, combined with some sort of absorptive mechanism. Stimulated by the expected results of PS185 several groups have studied the $\overline{Y}Y$ production reaction. This was done in 1984 by F. Tabakin and R. Eisenstein in their

extensive meson-exchange calculation of the $\overline{p}p \to \overline{\Lambda}\Lambda$ reaction [10]. A Born approximation method with improved initial- and final-state interactions was used. A delicate destructive interference between the $K^*(892)$ and $K_2^*(1430)$ exchanges was needed in order to describe the data. The importance of incorporating the K_2^* down to threshold was stressed. At the same time the $\overline{Y}Y$ channels were studied in Nijmegen by P. Timmers [7], using a full coupled-channels formalism, including quasi-two-body mesonic annihilation channels, similar to the one used in the Nijmegen model for low-energy antinucleon-nucleon scattering [11]. The existing bubble-chamber data from Jayet *et al.* [5] were described well by this model. It turned out to be surprisingly difficult to achieve a detailed fit to the data, mainly because of the very strong short-range strangeness-exchange tensor potential. Apart from this, there existed the obvious computational problem in dealing with many coupled channels (as many as 18 for each value of the isospin). In this work [7] the suppression of the $\overline{p}p \to \overline{\Lambda}\Lambda$ transition due to the strong final-state absorption and the importance of the strangeness-changing tensor force due to $K(494)$ and $K^*(892)$ exchange were demonstrated. Other OBE studies are the coupled-channels model of J. Niskanen [12] and the DWBA kaon-exchange model of M. Kohno and W. Weise [13]. The latter authors also demonstrated the presence of a substantial S-wave suppression due to the strong short-range absorption. For more recent studies of the reaction $\overline{p}p \to \overline{\Lambda}\Lambda$ using a DWBA approach see Refs. [14, 15].

All these studies emphasize the presence of strong initial- and final-state annihilation effects which call for a coupled-channels calculation. In earlier reports on our model [16, 17, 18] we have shown the dominant role of the tensor force in the $\overline{p}p \to \overline{\Lambda}\Lambda$ reaction, which accounts for the strong anisotropy of the differential cross section and the sizable polarization even close to threshold. In Ref. [16], where the model was applied to the first data taken by PS185 [1], we pointed out the need to use a good meson-exchange potential. In our case this potential is given by the Nijmegen soft-core nucleon-nucleon [19] and hyperon-nucleon [20] OBE potential, properly adapted via the C-parity transformation to the antibaryon-baryon channels. It is satisfactory to see that the same potential can account also very well for antibaryon-baryon scattering. The model was subsequently applied to the data [2] at one higher energy [17], and next to the data [3] taken very close to threshold [18].

Several quark model studies have been attempted, notably the $^3S_1$ pair creation model of M. Kohno and W. Weise [13] and the more extensive work of S. Furui and A. Faessler [21], which favors the $^3P_0$ pair creation model because it allows tensor-force transitions between $\overline{p}p$ and $\overline{Y}Y$. H. Rubinstein and H. Snellman [22] have given some theoretical justification for the use of perturbative QCD calculations at these low energies. An interesting alternative development is the diquark study of P. Kroll and W. Schweiger [23].

Ultimately both the meson-exchange and the quark-creation mechanism are probably present at the same time. The $K(494)$ and $K^*(892)$ potentials extend well beyond the inner region of the interaction, while short-ranged quark mechanisms may be hidden due to absorption in initial and final state. In view of these considerations, we present a model for describing antibaryon-baryon scattering in the LEAR momentum region that offers some clear advantages over other approaches. A coupled-channels partial-wave calculation using the multichannel Schrödinger equation is performed, taking into account all relevant baryonic channels. The interaction region is divided into two parts. A coupled-channels antibaryon-baryon meson-exchange potential is used in the outer region, which is connected to the

inner region with the use of the P-matrix formalism [24]. The short-range physics is treated phenomenologically. This allows us to incorporate initial- and final-state absorption properly and also to study the tail of the nuclear interaction. In particular the influence of the different strange mesons is investigated. This separation of very complex short-range and well-known long-range dynamics and the use of a meson-exchange potential of good quality allow an excellent description of the available data. We show how these data convincingly reflect the presence of a strong tensor force which is due to combined exchange of the $K(494)$ and $K^*(892)$ mesons.

The methods used in our model are in fact quite similar to the ones used in the Nijmegen phase-shift or partial-wave analyses of low-energy pp and np scattering data [25, 26]. We decided to present also a partial-wave analysis of all the low-energy $\overline{p}p \to \overline{\Lambda}\Lambda$ data taken at LEAR. We think that we are able to pin down reliably the behavior of the important transitions. We finally point out that this is the first time a multi-energy χ^2 fit is done to all the published LEAR data on the reaction $\overline{p}p \to \overline{\Lambda}\Lambda$.

The organization of this paper is as follows. Section 2 is devoted to the density-matrix formalism and the definition of the observables. In Section 3 we review the multichannel scattering and P-matrix formalism and explain its use in this particular scattering problem. Section 4 contains a description of the antibaryon-baryon potential and in Section 5 we present the results of the comparison of the model with the new LEAR data. Finally, in this section we perform a partial-wave analysis of the $\overline{p}p \to \overline{\Lambda}\Lambda$ data and present the corresponding 'model-independent' S-matrix elements. In appendix A we explain the SU(3)-flavor formalism, necessary for the derivation of the antibaryon-baryon potential, and in appendix B we derive a partial-wave decomposition of the relevant observables in $\overline{p}p \to \overline{\Lambda}\Lambda$.

II. DENSITY MATRIX FORMALISM AND OBSERVABLES

In this section we will briefly review the density-matrix formalism [27] applied to the $\overline{p}p \to \overline{Y}Y$ strong interaction, to the subsequent electroweak decay of the hyperons and its relation to the scattering observables: cross sections, polarizations, and spin correlations. To be specific the reaction $\overline{p}p \to \overline{\Lambda}\Lambda$ is taken as an example throughout the section. The initial $\overline{p}p$ state is described with a density matrix $\rho_{\overline{p}p}$ which is the outer product of the density matrices for the antiproton beam (with polarization $\mathbf{P}^{\overline{p}}$) and for the proton target (with polarization $\mathbf{P}^{p}$) and is thus given by

$$\rho_{\overline{p}p} = \frac{1}{4}(1 + \boldsymbol{\sigma}_{\overline{p}} \cdot \mathbf{P}^{\overline{p}}) \otimes (1 + \boldsymbol{\sigma}_{p} \cdot \mathbf{P}^{p}) \quad . \tag{1}$$

In case of scattering of an unpolarized beam on an unpolarized target we simply have

$$\rho_{\overline{p}p} = \frac{1}{4}\,(1 \otimes 1) \quad . \tag{2}$$

The strong interaction with amplitude M_s transforms this into the density matrix for the $\overline{\Lambda}\Lambda$ final state

$$\rho_{\overline{\Lambda}\Lambda} = M_s\ \rho_{\overline{p}p}\ M_s^{\dagger} \quad . \tag{3}$$

This scattering amplitude M_s is the quantity which is analyzed in our model. The density matrix $\rho_{\overline{\Lambda}\Lambda}$ can be expanded in the 16 basis matrices $\sigma_\mu^{\overline{\Lambda}} \otimes \sigma_\nu^{\Lambda}$, which are the outer products of the three Pauli matrices and $\sigma_0 = 1$

$$\rho_{\overline{\Lambda}\Lambda} = \frac{1}{4}\, I_0 \sum_{\mu,\nu} C_{\mu\nu}\, (\sigma_\mu^{\overline{\Lambda}} \otimes \sigma_\nu^{\Lambda}) \ . \tag{4}$$

Here $I_0 = d\sigma/d\Omega$, $C_{00} = 1$, $C_{i0} = P_i^{\overline{\Lambda}}$, $C_{0i} = P_i^{\Lambda}$, and C_{ij} are the spin-correlation coefficients. From the above expression for $\rho_{\overline{\Lambda}\Lambda}$ we can deduce easily

$$\begin{aligned} I_0 &= \mathrm{Tr}\ \rho_{\overline{\Lambda}\Lambda} \ , \\ I_0\ \mathbf{P}^{\Lambda} &= \mathrm{Tr}\ \rho_{\overline{\Lambda}\Lambda}\ \boldsymbol{\sigma}^{\Lambda} \ , \\ I_0\ \mathbf{P}^{\overline{\Lambda}} &= \mathrm{Tr}\ \rho_{\overline{\Lambda}\Lambda}\ \boldsymbol{\sigma}^{\overline{\Lambda}} \ , \\ I_0\ C_{ij} &= \mathrm{Tr}\ \rho_{\overline{\Lambda}\Lambda}\ \sigma_i^{\overline{\Lambda}} \otimes \sigma_j^{\Lambda} \ . \end{aligned} \tag{5}$$

Another useful observable is the so-called singlet fraction S defined by

$$\begin{aligned} I_0\ S = \mathrm{Tr}\ \rho_{\overline{\Lambda}\Lambda}\hat{S} &= \mathrm{Tr}\ \rho_{\overline{\Lambda}\Lambda}\frac{1}{4}(1 - \sigma^{\overline{\Lambda}} \otimes \sigma^{\Lambda}) \ = \\ &= \frac{1}{4}(1 - C_{xx} - C_{yy} - C_{zz}) \ , \end{aligned} \tag{6}$$

where the operator $\hat{S}$ projects out the singlet state. Analogously we can define the triplet fraction T

$$\begin{aligned} I_0\ T = \mathrm{Tr}\rho_{\overline{\Lambda}\Lambda}\hat{T} &= \mathrm{Tr}\rho_{\overline{\Lambda}\Lambda}\frac{1}{4}(3 + \sigma^{\overline{\Lambda}} \otimes \sigma^{\Lambda}) \ = \\ &= \frac{1}{4}(3 + C_{xx} + C_{yy} + C_{zz}) \ . \end{aligned} \tag{7}$$

It is obvious that $S + T = 1$. As to the kinematic limits on these observables we have that $-1 \leq P_i, C_{ij} \leq 1$ and $0 \leq S, T \leq 1$. When the spins of the outgoing particles are uncorrelated one has $S = \frac{1}{4}, T = \frac{3}{4}$.

It is customary to use a right-handed coordinate system in which the y-axis lies normal to the production plane and in which the z-axis is parallel to the direction of motion of the outgoing Λ (in the center-of-mass system). Using this set of axes and assuming the invariance of the strong interaction under the P and the C transformation separately one can prove important symmetry relations for the spin-observables. Applying conservation of parity it is easy to deduce that

$$\begin{aligned} P_x^{\Lambda} = P_z^{\Lambda} = P_x^{\overline{\Lambda}} = P_z^{\overline{\Lambda}} = 0 \ , \\ C_{xy} = C_{yx} = C_{yz} = C_{zy} = 0 \ . \end{aligned} \tag{8}$$

while charge-conjugation invariance adds the further restrictions

$$\begin{aligned} \mathbf{P}^{\Lambda} = \mathbf{P}^{\overline{\Lambda}} \ , \\ C_{ij} = C_{ji} \ , \end{aligned} \tag{9}$$

in case of self-charge-conjugate reactions (like $\overline{p}p \to \overline{Y}Y$). These symmetry relations leave us with five independent spin-observables: the polarization normal to the scattering plane P_y and the spin correlations C_{xx}, C_{yy}, C_{zz}, and C_{xz}, which are all functions of the center-of-mass scattering angle θ. From rotational invariance follow some simple relations. Both in the forward direction $\theta = 0$ and in the backward direction $\theta = \pi$ one has $P_y = 0$, $C_{xz} = 0$, and $C_{xx} = C_{yy}$.

Experimentalists usually give the observables using two different sets of body-fixed axes, $(x, y, z)_\Lambda$ and $(x, y, z)_{\overline{\Lambda}}$, which are rotated over 180° with respect to each other and where the z-axes are parallel to the momenta of the respective particles. This then gives a sign change in C_{xx}, C_{zz}, and C_{xz}. We will conform to this convention. It should be mentioned here that the data at $p_{\,\mathrm{lab}} = 1546.2$ MeV/c do not satisfy the requirement $C_{xx} = -C_{yy}$ at backward angles.

This completes the discussion of the strong interaction density-matrix formalism relevant for our theoretical model. For the sake of completeness we will say a few words on the experimental determination of these observables. After the production by the strong interaction the hyperons decay weakly (with the exception of the Σ^0). The experimentally detected charged decay modes in $\overline{p}p \to \overline{\Lambda}\Lambda$ are $\Lambda \to p\pi^-$ and $\overline{\Lambda} \to \overline{p}\pi^+$. The parity-breaking, CP-conserving weak interaction produces a density matrix

$$\rho_{p\pi^-} = M_w \, \rho_\Lambda \, M_w^\dagger \ , \tag{10}$$

where ρ_Λ is the density matrix for the polarized Λ hyperon

$$\rho_\Lambda = \frac{1}{2}(1 + \boldsymbol{\sigma}_\Lambda \cdot \mathbf{P}^\Lambda) \ . \tag{11}$$

Likewise for the decay $\overline{\Lambda} \to \overline{p}\pi^+$. Unlike the strong interaction amplitude M_s the form of the weak interaction amplitude M_w is known. From the observed angular distribution of the final-state decay products which is proportional to

$$M_w \, \overline{M}_w \, \rho_{\overline{\Lambda}\Lambda} \, \overline{M}_w^\dagger \, M_w^\dagger \tag{12}$$

the polarization and spin correlation of the $\overline{\Lambda}\Lambda$ system can be experimentally inferred. This is due to to the fact that the weak amplitude M_w contains a parity-breaking term. As a happy consequence, the weak decay produces a large asymmetry with respect to the polarization axes of the hyperons. Essentially this means that in the rest-system of the Λ the proton is not emitted isotropically, but that there is a preference on the part of the Λ to emit the proton in the direction of its polarization.

III. MULTICHANNEL SCATTERING FORMALISM

A. Multichannel Schrödinger Equation

Antiproton-proton scattering at intermediate energies is a complicated many channels problem. Consider this problem on the isospin basis. Restricting ourselves for the moment

to the two-particle antibaryon-baryon channels below 2.0 GeV/c momentum with isospin 0, 1, or 2, the following three scattering problems have to be solved

$$\begin{aligned} I=0: &\ (\overline{N}N, \overline{\Lambda}\Lambda, \overline{\Sigma}\Sigma) \to (\overline{N}N, \overline{\Lambda}\Lambda, \overline{\Sigma}\Sigma) \\ I=1: &\ (\overline{N}N, \overline{\Lambda}\Sigma + \overline{\Sigma}\Lambda, \overline{\Sigma}\Sigma) \to (\overline{N}N, \overline{\Lambda}\Sigma + \overline{\Sigma}\Lambda, \overline{\Sigma}\Sigma) \\ I=2: &\ (\overline{\Sigma}\Sigma) \to (\overline{\Sigma}\Sigma) \ . \end{aligned} \tag{13}$$

For isospin 0 or 1 the potentials on the isospin basis are 3×3 matrices in channel space (6×6 matrices in the case of tensor-force coupled partial waves). As an example for isospin 0 we get for the wave function and potential matrix

$$\Phi_0^J = \begin{pmatrix} \langle r\ell sJ|\overline{N}N\rangle \\ \langle r\ell sJ|\overline{\Lambda}\Lambda\rangle \\ \langle r\ell sJ|\overline{\Sigma}\Sigma\rangle \end{pmatrix} \ , \ V_0^J = \begin{pmatrix} V_{NN} & V_{N\Lambda} & V_{N\Sigma} \\ V_{\Lambda N} & V_{\Lambda\Lambda} & V_{\Lambda\Sigma} \\ V_{\Sigma N} & V_{\Sigma\Lambda} & V_{\Sigma\Sigma} \end{pmatrix} \ , \tag{14}$$

where the notation of the potential matrix elements is such that for instance $V_{\Lambda N} = \langle\overline{\Lambda}\Lambda|\ V\ |\overline{N}N\rangle$. Similar expressions hold for isospin 1. These potentials are used in the relativistic, symmetric version of the radial Schrödinger equation in channel space. The relativistic Schrödinger equation [28] is a differential form of the relativistic Lippmann-Schwinger integral equation, which in its turn is equivalent to three-dimensional relativistic integral equations like the Blankenbecler-Sugar equation [29]. For an isospin I partial wave with total angular momentum J we have

$$\left(\frac{d^2}{dr^2} \ - \ \frac{L^2}{r^2} \ - \ U_I^J \ + \ k^2\right) \Phi_I^J(r) \ = \ 0 \ . \tag{15}$$

Here $U_I^J = \sqrt{2m}\ V_I^J \sqrt{2m}$, where V_I^J denotes the coupled-channels antibaryon-baryon potential (see next section) and k and m are diagonal matrices containing the channel momenta (in the center-of-mass system) and reduced masses. The connection between the momenta k and the total center-of-mass energy $\sqrt{s}$ is given by the relativistic expression $k^2 = \frac{1}{4}s - m^2$ (for equal baryon masses). L^2 is a diagonal matrix with entries $\ell(\ell+1)$. In order to have the correct thresholds and to be able to include the Coulomb interaction we use the physical particle basis in our calculation. Taking into account all baryonic channels below 2.0 GeV/c antiproton momentum, there are 7 coupled channels for partial waves with $\ell = J$, $s = 0, 1$ and 14 coupled channels for tensor-force coupled partial waves with $\ell = J \pm 1$, $s = 1$.

B. The P matrix

Up to this point only the two-body baryonic channels have been accounted for, but the many mesonic annihilation channels coupled to the $\overline{p}p$ system have not been included yet. In these baryonic channels the long-range interaction is in our model given by an antibaryon-baryon meson-exchange potential. For the complicated short-range interaction we think that the meson-exchange picture is perhaps of limited use, since here the physics is probably dominated by a strong coupling to the many annihilation channels and possibly by quark and gluon degrees of freedom. With the help of the so-called P-matrix formalism [24] we

will circumvent the problem of the complex short-range physics. The P matrix is defined as the logarithmic derivative of the solution matrix $\Phi(r)$ at a distance $r = b$ from the origin

$$P(k,b) \;=\; b\left(\frac{d\Phi}{dr}\Phi^{-1}\right)_{r=b} \quad , \tag{16}$$

where the factor b is included in the definition in order to make the P matrix dimensionless. In the original work the P matrix was used by Jaffe and Low in the bag model where at the energies of the eigenstates of the confined quark and gluon degrees of freedom the P matrix exhibits poles. More generally the P matrix relates the inner to the outer region physics. In scattering problems the short-range interaction is largely unknown and has to be treated phenomenologically. The long-range physics is much better understood theoretically. The P-matrix formalism provides a useful separation between these two regions and is a very powerful tool in analyzing scattering data. Recently the P matrix has proven its power in the Nijmegen partial-wave analyses of nucleon-nucleon scattering data [25, 26]. As already mentioned in the introduction, using the same techniques here we can determine quite reliably the behavior of the most important amplitudes.

We have put the boundary b at 1.2 fm. Any value between about 1.1 fm and 1.3 fm would allow us to get an almost equally good fit to the data but 1.2 fm is more or less the optimal value. This is closely related to the range of the annihilation potential. Outside $r = b$ a (real) meson-exchange potential is used, whereas the (imaginary) annihilation potential inside $r = b$ is completely represented by the P matrix (see next section). This shows that the annihilation potential is of intermediate range because if we take the boundary at values smaller than 1 fm it is impossible to fit the data on $\overline{p}p \to \overline{p}p$ in a proper way. In particular it would be very difficult to achieve a reasonable fit to the forward diffraction peak and minimum present in the elastic differential cross section.

Starting with the boundary condition (16) we integrate the matrix equation (15) numerically for each partial wave with $J \leq J_{\rm max}$ up to a distance r_∞ well beyond the range of the nuclear potential (we use $r_\infty = 12.0$ fm). There the S matrix is evaluated by matching $\Phi(r_\infty)$ to Coulomb or spherical Hankel functions. All the scattering observables defined in the previous section can then be calculated using standard methods.

C. Parametrization of the P matrix

In the previous subsection we explained how the complicated short-range interaction can be represented by the P-matrix boundary condition on the wave function. The P matrix has to be parametrized in a phenomenological manner. Many different parametrizations are possible. Let us begin the discussion with single-channel scattering. A simple but very convenient choice for the short-range interaction is a square-well potential of range b. The P matrix for a single-channel square-well problem in a partial wave with orbital angular momentum ℓ is given by

$$P_\ell(k,b) \;=\; k'b\,\frac{J'_\ell(k'b)}{J_\ell(k'b)} \quad , \tag{17}$$

where $J_\ell(z) = z j_\ell(z)$ with $j_\ell(z)$ the spherical Bessel function and $k'^2 = k^2 - 2mV$, V being the depth of the square-well potential. The prime on the Bessel function denotes differentiation with respect to the argument. The many mesonic annihilation channels which are coupled to each single antibaryon-baryon channel through a short-range annihilation potential are taken into account as an average by using a complex square well, leading to a complex instead of a real P matrix.

The simplest way to treat the case of coupled channels is to start from these single-channel P matrices (which of course are just complex numbers) and arrange them in a diagonal matrix. The next step is to specify some sort of coupling. The short-range coupling between different antibaryon-baryon channels and the coupling due to the tensor force are taken into account by adding a prescription to parametrize the off-diagonal P-matrix elements. Suppose we have a diagonal P matrix for two coupled channels. A useful construction to describe the mixing between these channels, and the one we will actually employ in our model is given by

$$P = \begin{pmatrix} \cos\theta & \sin\theta \\ -\sin\theta & \cos\theta \end{pmatrix} \begin{pmatrix} P_1 & 0 \\ 0 & P_2 \end{pmatrix} \begin{pmatrix} \cos\theta & -\sin\theta \\ \sin\theta & \cos\theta \end{pmatrix} \quad . \tag{18}$$

In general the angle θ can be parametrized as a function of energy, although in our calculation we can take it a constant, dependent on the partial wave.

In this way we have finally arrived at a multichannel P matrix. The fact that a complex annihilation potential is used in the parametrization means that the corresponding P matrix is no longer hermitean, though still symmetric. This last fact follows from time-reversal invariance, which allows us to choose the phases of our physical states in such a way that the potential matrix and consequently the P matrix is symmetric. This gives us

$$P_J^T(k,b) = P_J(k,b) \quad , \quad P_J^\dagger(k,b) \neq P_J(k,b) \quad , \tag{19}$$

where the T denotes transposition in channel space. For the partial-wave S matrix we then get

$$S_J^T(k) = S_J(k) \quad , \quad S_J^\dagger(k) \neq S_J^{-1}(k) \quad . \tag{20}$$

The fact that the S matrix is not unitary accounts for the disappearance of probability (flux) into the mesonic channels.

IV. ANTIBARYON-BARYON POTENTIAL

In this section we want to sketch the derivation of the antibaryon-baryon potential to be used in the multichannel Schrödinger equation discussed in the previous section. In keeping with the work of the Nijmegen group on nucleon-nucleon and hyperon-nucleon potentials [19, 20], we will assume that flavor SU(3) holds for the coupling constants between baryons and mesons. In order to implement this assumption and to calculate the various isospin symmetry factors, it is convenient to start the discussion from a Lagrangian of baryons and mesons with unbroken flavor symmetry, where the hadrons are assigned to multiplets which transform according to definite irreducible representations of SU(3). The formalism used

here to describe the mutual interaction of baryons and mesons is explained in appendix A to which we refer for details.

Out of the baryon and meson fields direct products can be formed with the help of the (real) SU(3) Clebsch-Gordan coefficients [30]. This procedure leads to a local interaction Lagrangian of the following general form

$$\mathcal{L}_{int}(x) = -\sum_{\gamma\nu\nu_1\nu_2} g(\gamma) \begin{pmatrix} \mu_1 & \mu & \mu_{2_\gamma} \\ \nu_1 & \nu & \nu_2 \end{pmatrix} \overline{\psi}^{(\mu_2)}_{\nu_2}(x)\; i\Gamma\; \psi^{(\mu_1)}_{\nu_1}(x) \phi^{(\mu)}_{\nu}(x) \quad . \tag{21}$$

The reader may easily verify that this interaction Lagrangian is a flavor singlet. The form (21) is equivalent to the more familiar one which is obtained by constructing a baryon current out of $\psi(x)$ and $\overline{\psi}(x)$ and coupling this current with the meson field $\phi(x)$ to a flavor singlet. In the expression for $\mathcal{L}_{int}$ only flavor indices are explicitly shown whereas Dirac spinor and Lorentz space-time indices as well as possible derivatives acting on the baryon and meson fields are suppressed. $i\Gamma$ is an SU(3) invariant operator, for example a Dirac matrix in spinor space. Taking into account meson multiplets of different spin and parity we distinguish in our model scalar, pseudoscalar, vector, and tensor mesons. The interaction Lagrangians for these exchanges are summarized in Table II where this time the flavor indices and summations are suppressed.

We apply this formalism to the case of antibaryon-baryon scattering $\overline{B}_1 B_2 \to \overline{B}_3 B_4$. In doing this care has to be taken with the phases of the antibaryon multiplet with respect to the baryon multiplet. In order to make the calculation more transparent as well as to keep track of these phase factors a set of Feynman rules, derived using the conventions of appendix A, is given in Table III.

Evaluating the one-boson-exchange diagram for $\overline{B}_1 B_2 \to \overline{B}_3 B_4$ with the help of these rules gives for the scattering amplitude

$$\begin{aligned} M_{fi} &= \langle \mu_3^* \nu_3 \mu_4 \nu_4 \,|M|\, \mu_1^* \nu_1 \mu_2 \nu_2 \rangle \quad = \\ &= -\sum_{\gamma\gamma'\nu} g_{13}(\gamma) g_{24}(\gamma') \begin{pmatrix} \mu_1^* & \mu & \mu_{3_\gamma}^* \\ \nu_1 & -\nu & \nu_3 \end{pmatrix} \begin{pmatrix} \mu_2 & \mu & \mu_{4_{\gamma'}} \\ \nu_2 & \nu & \nu_4 \end{pmatrix} \\ &\quad \times [\overline{u}(4)\,\Gamma\,u(2)]\; iD_F(k)\; [\overline{v}(1)\,\Gamma\,v(3)] \quad , \end{aligned} \tag{22}$$

in an obvious notation. The indices μ and ν denote the flavor SU(3) quantum numbers of the exchanged meson. $D_F(k)$ is the Feynman propagator for the exchanged meson, for a scalar or pseudoscalar meson given by $iD_F(k) = (k^2 + m^2 - i\varepsilon)^{-1}$. Although we will not use it here, we mention for completeness that with these conventions the baryon propagator reads $iS_F(p) = (i\gamma \cdot p + m - i\varepsilon)^{-1}$.

As far as the masses of the baryons and mesons are concerned, flavor SU(3) symmetry is of course broken in nature and this breaking of the mass degeneracy can very easily be incorporated. Maintaining for the moment SU(2)⊗U(1) isospin-hypercharge symmetry, contained in SU(3), let us calculate the scattering amplitude on the isospin basis. To achieve this we split the SU(3) Clebsch-Gordan coefficient in the product of a SU(2) Clebsch-Gordan coefficient and a so-called isoscalar factor [30] in the standard way

$$\begin{pmatrix} \mu_1 & \mu_2 & \mu_{3_\gamma} \\ \nu_1 & \nu_2 & \nu_3 \end{pmatrix} = C \begin{pmatrix} I_1 & I_2 & I_3 \\ m_1 & m_2 & m_3 \end{pmatrix} \left(\begin{array}{cc|c} \mu_1 & \mu_2 & \mu_{3_\gamma} \\ I_1 Y_1 & I_2 Y_2 & I_3 Y_3 \end{array} \right) \quad . \tag{23}$$

Furthermore we take initial and final two-particle states of definite isospin and hypercharge obtained from the direct products of the one-particle states with SU(2) Clebsch-Gordan coefficients. The scattering amplitude can be written in the following compact form

$$M_{fi} = \langle \mu_3^* I_3 Y_3 \mu_4 I_4 Y_4 I^{'} Y^{'} m^{'} \; |M| \; \mu_1^* I_1 Y_1 \mu_2 I_2 Y_2 I Y m \rangle \quad = \tag{24}$$

$$= -\delta_{II'}\delta_{YY'}\delta_{mm'} \sum_{I^{''}Y^{''}} G(IY; I^{''}Y^{''}) \; [\overline{u}(4)\,\Gamma\,u(2)] \; iD_F(k) \; [\overline{v}(1)\,\Gamma\,v(3)] \quad ,$$

where $I^{''}$ and $Y^{''}$ are the isospin and the hypercharge of the exchanged meson. The factors $G(IY; I^{''}Y^{''})$ in this expression read

$$G(IY; I^{''}Y^{''}) \; = \sum_{\gamma\gamma'} g_{13}(\gamma) g_{24}(\gamma') \left(\begin{array}{cc|c} \mu & \mu_3^* & \mu_{1_\gamma}^* \\ I^{''}Y^{''} & I_3 Y_3 & I_1 Y_1 \end{array} \right)$$

$$\times \left(\begin{array}{cc|c} \mu_2 & \mu & \mu_{4_{\gamma'}} \\ I_2 Y_2 & I^{''}Y^{''} & I_4 Y_4 \end{array} \right) \left[\begin{array}{ccc} I_2 & I^{''} & I_4 \\ 0 & I_3 & I_3 \\ I_2 & I_1 & I \end{array} \right] \quad , \tag{25}$$

with the help of an SU(2) 9-j symbol. In order to arrive at this specific form, we employed some symmetry relations [30] for the Clebsch-Gordan coefficients and isoscalar factors, valid for baryon octets and meson octets and singlets. The factors $G(IY; I^{''}Y^{''})$ given in (25), expressed in terms of the baryon-meson coupling constants are collected in Table IV for the case of pseudoscalar meson exchange. They were evaluated using the numerical values for the isoscalar factors given in [30]. In the Table the isosinglet η is actually the octet member η_8. The flavor singlet η_1 couples universally to all members of the baryon octet. The physical nonet members η and η' are mixtures of η_8 and η_1.

In the same manner as shown above the SU(2)⊗U(1) symmetry can be broken further in order to account for the mass differences within each isospin multiplet. This is what we do in our calculation since otherwise the different $\overline{\Sigma}\Sigma$ thresholds would still remain degenerate. For completeness we give the relation between the coupling constants $g(\gamma)$ $(\gamma = 1, 2)$ used here and the F and D type couplings found in literature

$$g(1) = -\sqrt{\frac{20}{3}}(\alpha - 1) g \quad , \quad g(2) = 2\sqrt{3}\alpha \, g \quad , \tag{26}$$

where α is the $F/(F+D)$ ratio and g is for example the pion-nucleon coupling constant $g_{NN\pi}$ in case of pseudoscalar mesons. All baryon-meson coupling constants can be expressed in terms of g and α. As an example, for the strange mesons we have

$$f_{\Lambda NK} = -f(1 + 2\alpha)/\sqrt{3} \quad , \quad f_{\Sigma NK} = f(1 - 2\alpha) \quad , \tag{27}$$

where SU(3) flavor symmetry is assumed for the pseudovector coupling constant (so $f = f_{NN\pi}$).

To make contact, at last, with the baryon-baryon OBE potential, we have to relate the factor $[\overline{v}(1)\,\Gamma\,v(3)]$ to the corresponding factor $[\overline{u}(3)\,\Gamma\,u(1)]$ which occurs in the analogous expression in baryon-baryon scattering. Some gymnastics using properties of the Dirac spinors and gamma matrices reveals that this relation is provided by the C parity of the neutral member ϕ^0 of the meson multiplet in the following way

$$[\overline{v}(1)\,\Gamma\,v(3)] = -(-)^{C(\phi^0)}[\overline{u}(3)\,\Gamma\,u(1)] \quad . \tag{28}$$

This relation leads to a connection between the potentials for the two reactions $\overline{B}_1 B_2 \to \overline{B}_3 B_4$ and $B_3 B_2 \to B_1 B_4$ where the same meson is exchanged

$$V(\overline{B}_1 B_2 \to \overline{B}_3 B_4) = (-)^{C(\phi^0)} V(B_3 B_2 \to B_1 B_4) \quad . \tag{29}$$

For instance we have that

$$\begin{aligned} V(\overline{p}p{\to}\overline{p}p) &= V(pp{\to}pp) \quad \text{for} \;\; \pi^0 \;\; \text{exchange}, \\ V(\overline{p}p{\to}\overline{n}n) &= V(np{\to}pn) \quad \text{for} \;\; \pi^+ \;\; \text{exchange}, \\ V(\overline{p}p{\to}\overline{\Lambda}\Lambda) &= V(\Lambda p{\to}p\Lambda) \quad \text{for} \;\; K^+ \;\; \text{exchange}. \end{aligned}$$

We remark that, in case one works on the physical particle basis, it is simpler to use the C-parity transformation instead of the well-known G-parity rule. Finally, the non-relativistic reduction of the Dirac spinors and a Fourier transformation to configuration space leads in a standard way to the meson-exchange potentials.

It is important that in the outer region a realistic potential of good quality is used. The meson-exchange potential we use is the Nijmegen soft-core hyperon-nucleon OBE potential [20]. Our description of the intermediate- and long-range interaction is thus parameter-free. This OBE soft-core potential based on the Regge-pole nature of the mesons [19] gives a very good description of the existing data on NN and YN scattering. The following meson nonets are taken into account:

- The $J^{PC} = 0^{-+}$ pseudoscalar-meson nonet (π, η, η', K). SU(3) symmetry is assumed for the pseudovector coupling constant f.
- The $J^{PC} = 1^{--}$ vector-meson nonet $(\rho, \phi, \omega, K^*)$.
- The $J^{PC} = 0^{++}$ scalar-meson nonet $(a_0(980), f_0(975), f_0'(760), K_0^*(1000))$.
- The $J^{PC} = 2^{++}$ tensor-meson nonet $(a_2, f_2, P \oplus f_2', K_2^*)$. Actually only the 'diffractive' $J^{PC} = 0^{++}$ contribution from the tensor Regge trajectory is taken, leading to effective scalar-like potentials. This also leads to a mixing between the Pomeron P and the unitary singlet f_2'. In the Nijmegen potential the Pomeron is an important ingredient. It should be noted that F. Low and S. Nussinov have demonstrated [31] in the context of QCD that Pomeron-exchange can be viewed as a two-gluon-exchange effect.

The explicit potential functions as well as the numerical values of all the coupling constants and other parameters can be found in [20]. Gaussian form factors are used at the vertices, reflecting the quark structure of the hadrons. The coupling constants of the strange mesons at the ΛN and ΣN vertices, of particular interest to our problem, are summarized in Table V.

Some further remarks regarding details of our use of this baryon-baryon potential have to be made. First of all, the non-local terms of the potential are neglected because they cannot be handled in the Schrödinger equation with the same method as used in NN and YN models [32]. Simply leaving these short-range terms out is a very good approximation outside 1.2 fm where the OBE potential is used. Secondly, charge-symmetry breaking [33, 34] is included and introduces a mixing between π^0 and η and between Λ and Σ^0. It leads for instance to a long-range one-pion-exchange potential in $\overline{\Lambda}\Lambda \to \overline{\Lambda}\Lambda$ scattering.

Some general features of the resulting potential are the following. Very attractive potentials are present in the elastic channels due to the coherence of ω and f_0' exchanges. In the $\overline{p}p \to \overline{\Lambda}\Lambda$ reaction we get a very strong tensor force from the combined K and K^* exchanges. The spin-spin potentials of these mesons have opposite sign, whereas their tensor potentials have the same sign. Compare this to the case of charge-exchange $\overline{p}p \to \overline{n}n$ scattering where the tensor potentials due to π and ρ exchange also add up. The five different potential forms, central V_C, spin-spin V_{SS}, tensor V_T, spin-orbit V_{SO}, and quadratic spin-orbit V_Q, for this reaction are shown in Figure 1. We finally remark that in this way we do not, to this order in the coupling constant, get a potential for the double-charge-exchange reaction $\overline{p}p \to \overline{\Sigma^-}\Sigma^-$ [35] and the double-strangeness-exchange cascade production reactions $\overline{p}p \to \overline{\Xi^0}\Xi^0$ and $\overline{p}p \to \overline{\Xi^-}\Xi^-$. These reactions are mediated via πK and $2K$ exchange. They can however be treated analogously using the formalism outlined above. We want to point out, however, that in a multichannel calculation the transition $\overline{p}p \to \overline{\Sigma^-}\Sigma^-$ is automatically obtained as a two-step process, for instance $\overline{p}p \to \overline{\Lambda}\Lambda \to \overline{\Sigma^-}\Sigma^-$ via subsequent $K^\pm$ and $\pi^\pm$ exchange. The reaction $\overline{p}p \to \overline{\Xi^0}\Xi^0$ can be generated for instance via $\overline{p}p \to \overline{\Sigma^+}\Sigma^+ \to \overline{\Xi^0}\Xi^0$ through K^0 and $K^\pm$ exchange. The relative importance of this mechanism involving only OBE forces as compared to a direct transition via πK or $2K$ exchange needs to be investigated.

We have taken everywhere the linear combination $\overline{\Lambda}\Sigma^0 + \overline{\Sigma^0}\Lambda$ and disregarded the orthogonal $\overline{\Lambda}\Sigma^0 - \overline{\Sigma^0}\Lambda$ state, because the latter does not couple to the $\overline{N}N$ system. The C parity of a $\overline{N}N$ state with orbital angular momentum ℓ and spin s is given by $(-)^{\ell+s}$. This state can couple to a $\overline{\Lambda}\Sigma^0 + \overline{\Sigma^0}\Lambda$ state which has the same C parity. The orthogonal state $\overline{\Lambda}\Sigma^0 - \overline{\Sigma^0}\Lambda$ has C parity $(-)^{\ell+s+1}$.

V. RESULTS, DISCUSSION, AND OUTLOOK

A. Elastic scattering $\overline{p}p \to \overline{p}p$

With our model we will now analyze the scattering data on $\overline{p}p \to \overline{p}p$ and $\overline{p}p \to \overline{\Lambda}\Lambda$ recently taken at LEAR. Previous studies by others and ourselves have almost without exception pointed out the importance of initial- (and final-) state interaction effects on the antihyperon-hyperon pair production reaction. These should be taken into account properly. In this subsection we will consider the case of elastic $\overline{p}p \to \overline{p}p$ scattering. At these intermediate energies from 1.5 up to 2.0 GeV/c antiproton laboratory momentum elastic scattering occurs mainly in D, F, and G waves, with many partial waves of both isospin 0 and 1 substantially contributing. To the charge-exchange reaction $\overline{p}p \to \overline{n}n$, data on which are unfortunately almost completely lacking at these energies, even more transitions contribute significantly. The data on $\overline{p}p \to \overline{p}p$ consist of total and elastic cross sections, very accurate differential cross

sections of Eisenhandler *et al.* [36], and high-quality asymmetry data of Kunne *et al.* [37, 38], also recently obtained at LEAR by the PS172 collaboration. We are able to achieve a nice fit to these data, an example of which is shown in Figure 2 for the differential cross section at 1500 MeV/c, fitted with $\chi^2/\text{data} = 1.5$, and for the asymmetry at 1550 MeV/c, fitted with $\chi^2/\text{data} = 1.5$. Especially the characteristic diffraction peak of the forward cross section is nicely reproduced. In subsection 3.2 we remarked that this is connected to the range taken for the annihilation potential. In our model this range is determined by the position of the boundary. The value $r = b = 1.2$ fm gives the best results.

The fit is done with only one imaginary annihilation potential parameter used in all partial waves of both isospins. Furthermore we need 10 real potential parameters, 5 for each isospin. Most of these parameters are necessary to obtain a satisfactory result for the asymmetry. With more parameters the fit could be even better, but it is not our main objective to fit the elastic data. If we were to look only at the cross sections, fewer parameters would suffice. Moreover, it is important to note that with the exception of the annihilation parameter to take care of the necessary amount of annihilation, these parameters are not essential for the quality of the fit to the data on $\overline{p}p \to \overline{\Lambda}\Lambda$. It is only the long-range interaction in the initial state (which has no free parameters) that is relevant for the strangeness-exchange reactions. This is shown by the fact that with no short-range elastic potential apart from one annihilation parameter an excellent fit to the data on $\overline{p}p \to \overline{\Lambda}\Lambda$ is possible. We can understand this physically since the most important transitions start in the D-, F-, and G-wave $\overline{p}p$ channels. It thus appears that we do not need to specify the short-range initial-state interaction. In order to concentrate on the $\overline{p}p \to \overline{\Lambda}\Lambda$ data and to minimize the number of parameters we will continue with the parameter set where we have only one parameter for the initial state.

B. Strangeness-exchange scattering $\overline{p}p \to \overline{\Lambda}\Lambda$

In order to discuss the reaction $\overline{p}p \to \overline{\Lambda}\Lambda$ we have to specify some sort of prescription for the final-state interaction. Of course no data exist on the reaction $\overline{\Lambda}\Lambda \to \overline{\Lambda}\Lambda$, so that essentially nothing is known about the final-state beyond what can be inferred from SU(3) symmetry considerations. Contrary to the initial state here the short-range interaction is quite important. The available kinetic energy in the $\overline{\Lambda}\Lambda \to \overline{\Lambda}\Lambda$ channel is low and scattering occurs mainly with the $\overline{\Lambda}\Lambda$ system in S and P waves (with a rapid rise of D-wave contributions). The final-state absorption, again one imaginary potential parameter for all partial waves, is important in scaling the total cross section for the reaction $\overline{p}p \to \overline{\Lambda}\Lambda$. Three real parameters for the short-range potential in the final state are needed, one for the $^3S_1$ wave, one for the $^3P_2$ wave, and one for all other partial waves. With only these 5 initial- and final-state parameters, already a reasonable fit is possible to the data on $\overline{p}p \to \overline{\Lambda}\Lambda$, with a $\chi^2/\text{data} = 3.0$. This clearly shows the importance of the initial- and final-state interactions, which determine the global features of the data in a qualitative way. It also shows the quality of the the long-range Nijmegen potential tail, especially the off-diagonal strangeness-changing part.

The differential cross sections exhibit a typical behavior at almost all energies, namely a peak at forward angles, followed by a more or less flat backward cross section. This already shows that a large amount of scattering occurs at longer range, in P or higher waves, even

at energies very close to threshold ($\varepsilon \leq 5$ MeV). The polarizations are positive at forward angles, go through zero and stay negative at backward angles; except at very low energies where the polarization is positive over the entire angular range. The break in the differential cross section and the zero in the polarization occur at all energies at approximately the same value of momentum-exchange $t' = t - t_{\rm min}$ in the center-of-mass system. Also the minimum in the diffraction peak in $\overline{p}p \to \overline{p}p$ occurs at about the same place. In a simple picture of absorptive scattering the mean value of the slope of the forward differential cross section corresponds to scattering off a disk with radius $r = 1.2$ fm.

Available are data at six energies, at the highest energy enough events were measured to infer also the spin correlations. To describe these data quantitatively, we have to specify some parameters that correspond to short-range couplings between $\overline{p}p$ and $\overline{\Lambda}\Lambda$. As explained in detail in section 3.3 this can be done by parametrizing the off-diagonal P-matrix elements with the help of mixing angles according to equation 18. An excellent fit is obtained to the data-set with the introduction of only five off-diagonal mixing parameters describing the short-range coupling between two channels. We need mixing angles in the following transitions: ${}^3S_1$, ${}^3P_2$, ${}^3D_3$, and the three lowest tensor-force transitions: ${}^3D_1 \to {}^3S_1$, ${}^3F_2 \to {}^3P_2$, and ${}^3G_3 \to {}^3D_3$. The parameter for the ${}^3D_1 \to {}^3S_1$ transition can be taken equal to the one for the ${}^3S_1$ transition. The fit is slightly improved by parametrizing the other triplet P transitions with the same parameters as the ${}^3P_2$ transition. Transitions with $\ell \geq 3$ or in singlet states are not parametrized as the data are not sensitive to these parameters. The parameter set is summarized in Table VI, where we also give the 'errors' on the parameters, defined in the usual way as the change in each parameter which gives a maximal rise in the total $\chi^2_{\rm min}$ of 1.0 when the remaining parameters are refitted. These errors measure how sensitive the fit is to the inclusion of a certain parameter. Note that the mixing angles are quite small.

The results for this parameter set are given in Table VII for the different groups of data. The final fit has $\chi^2_{\rm min} = 180.6$ for a set of 157 data, this means $\chi^2/{\rm data} = 1.15$. If we look at the different observables we see that the 99 cross sections are fitted with $\chi^2_{\rm min} = 106.2$ ($\chi^2/{\rm data} = 1.07$), 38 polarizations with $\chi^2_{\rm min} = 37.9$ ($\chi^2/{\rm data} = 1.00$), and 20 spin correlations with $\chi^2_{\rm min} = 36.5$ ($\chi^2/{\rm data} = 1.83$). It should be mentioned that 2 out of 5 data-points for C_{zz} are outside their kinematically allowed boundaries, being more negative than -1. Also we see from Figure 5 that the spin-correlation data do not satisfy the restriction $C_{xx} = -C_{yy}$ at backward angles following from rotational invariance (see section 2). Our model of course does satify this restriction. A few data were not included in the fit, first of all the 5 polarizations at 1435.95 MeV/c ($\varepsilon = 0.24$ MeV), since they give essentially the same information as those at 1436.95 MeV/c ($\varepsilon = 0.59$ MeV) and are of somewhat less quality. Also one cross section and one polarization point were left out because of their abnormal high contribution to $\chi^2_{\rm min}$. These 7 data-points are not included in the final data-set for which we quote the results.

The results for the different observables at the different energies are summarized in Table VII. The integrated cross sections $\sigma_{\overline{\Lambda}\Lambda}$ were not included, because they are redundant and should follow from integrating the differential cross sections. We tabulate also the rejected data and the theoretical normalizations with which the model results should be multiplied before comparing them to the data. A 5% normalization error was assumed for all data. As can be seen from this Table the overall picture is quite good with the possible

exception of the observable C_{zz}. A large negative value of C_{zz} means that the antihyperon-hyperon pair is produced mostly with opposite helicities. Here there is perhaps room for improvement with the help of data at higher energies. From the Table we see that there is a (slight) normalization problem with the differential cross section at 1476.5 MeV/c ($\varepsilon = 14.5$ MeV).

The resulting fits at four energies are shown in Figures 3 to 5. Partial cross sections at six energies are tabulated in Table VIII. The dominance of the tensor-force induced transitions even at low energies is immediately evident. We remind the reader that the threshold ($\varepsilon = 0$ MeV) of the $\overline{p}p \to \overline{\Lambda}\Lambda$ reaction lies at $p_{\,\mathrm{lab}} = 1435.07$ MeV/c, and that the lowest energy at which data were taken corresponds to $p_{\,\mathrm{lab}} = 1435.95$ MeV/c ($\varepsilon = 0.24$ MeV). The important ${}^3P_2$, ${}^3P_1$, and ${}^3F_2 \to {}^3P_2$ transition are the cause of the non-zero polarization close to threshold and their interference with the ${}^3S_1$ and ${}^3D_1 \to {}^3S_1$ transition explains the anisotropy of the differential cross section at these energies. The combined tensor-force transitions $\ell(\overline{\Lambda}\Lambda) = \ell(\overline{p}p) - 2$ make up 90% of the total cross section at $p_{\,\mathrm{lab}} = 1435.95$ MeV/c ($\varepsilon = 0.24$ MeV), and still 56% at $p_{\,\mathrm{lab}} = 1546.2$ MeV/c ($\varepsilon = 39.1$ MeV).

The S- and P-wave contributions to the integrated cross section close to threshold are shown in Figure 6. The data here are from [3, 39]. The P waves start to dominate the S waves at very low values of ε. Also apparent (from Table VIII) is the dominance of scattering in triplet states, the singlet fraction being practically zero everywhere, even to such an extent that it is possible to speak of a dynamical selection rule. Again this is mainly due to the contribution of the tensor-force transitions.

Concerning the importance of the different strange mesons, the following can be said. The model is not very sensitive to inclusion of the scalar K_0^* and tensor K_2^* mesons, but the strong K^* potential has a large influence on the parameters, and should of course be included in any realistic potential model. Also quantitatively we can see this. If we leave out the K^* completely and refit the parameters, χ^2_{min} rises by 5.0. As can be seen from Figure 1 the scalar-like K_2^* potential is quite weak. If we were to include the full tensor-meson-exchange potential, instead of just its $J = 0$ diffractive piece, it is not difficult to see from Section 4 that the resulting potential would contain a tensor force again of the same sign as those of the K and K^* exchanges. So, in general, from a OBE model one gets a strong short-range strangeness-changing tensor potential, which would in fact in a full coupled-channels potential model where meson-exchange forces are taken into account at all distances down to $r = 0$ pose some problems in achieving a very good fit to the data [7].

In hindsight, the dominance of the tensor-force transitions can be understood using the following simple argument. The transition probability is in the first Born approximation maximal when the wave function overlap is maximal. In the case of free spherical Bessel functions $prj_\ell(pr)$ this maximum lies at $r \sim \sqrt{\ell(\ell+1)}/p$. In our case $p_{\overline{\Lambda}\Lambda}$ is much smaller than $p_{\overline{p}p}$, so the overlap is maximal when $\ell_{\overline{\Lambda}\Lambda}$ is smaller than $\ell_{\overline{p}p}$. These transitions are moreover favored by the presence, in $\overline{p}p \to \overline{\Lambda}\Lambda$, of a very strong tensor force due to the coherent exchange of the K and K^* mesons.

Dalkarov, Protasov, and Shapiro [41] recently explained the specific features of the data on $\overline{p}p \to \overline{\Lambda}\Lambda$ with the use of so-called P-wave 'enhancements'. This phenomenon, caused by narrow resonances, was invoked to explain the substantial P-wave contributions to the cross sections at low energies. Tensor forces, however, were not included in order to simplify the

calculations. In view of the results obtained with our model this seems a very unrealistic approach. Our calculation clearly shows that in a coupled-channels model that takes the tensor force properly into account, there is absolutely no need to resort to exotic things like enhanced P waves. Rather there is suppression of both S- and P-wave transitions due to short-range annihilation and in particular of the S-wave transitions (for which there is no centrifugal barrier).

Several trends in the data can be nicely understood using a partial-wave decomposition of the observables [42] which is derived in appendix B. This decomposition allows one to see the effects of certain transitions. Of course this is best done close to threshold where only S and P waves contribute to the scattering proces. If more waves contribute the results are no longer so transparent. Let us first take the case where the only transitions contributing significantly are ${}^3S_1 \to {}^3S_1$ and ${}^3D_1 \to {}^3S_1$. As can be seen from Table VIII this is the case only at very low energies above threshold. Even at $p_{\rm lab} = 1435.95$ MeV/c ($\varepsilon = 0.24$ MeV) there is some P-wave scattering. However, it interesting to see how the different observables start out at threshold. The polarization is zero in this case, and the spin correlations have the following shape

$$
\begin{aligned}
C_{xx}(\theta) &= -\frac{1}{4}\mathcal{C}_1 \cos 2\theta - \frac{1}{2}\mathcal{C}_2 \sin^2\theta \quad , \\
C_{yy}(\theta) &= \frac{1}{4}\mathcal{C}_1 \quad , \\
C_{zz}(\theta) &= \frac{1}{4}\mathcal{C}_1 \cos 2\theta - \frac{1}{2}\mathcal{C}_2 \cos^2\theta \quad , \\
C_{xz}(\theta) &= -\frac{1}{4}\mathcal{C}_1 \sin 2\theta + \frac{1}{4}\mathcal{C}_2 \sin^2\theta \quad ,
\end{aligned}
$$

where the constants read $\mathcal{C}_1 = |S_1 + \sqrt{2}C_1|$ and $\mathcal{C}_2 = |S_1 - \frac{1}{2}\sqrt{2}C_1|$. S_1 and C_1 denote the matrix elements $\langle f\ell'|(S^J - 1)|\ell i\rangle/2ik$ for the ${}^3S_1$ and ${}^3D_1 \to {}^3S_1$ transitions respectively (see appendix B). Looking at Figure 5, we see that at $p_{\rm lab} = 1445.35$ MeV/c the shape of the spin correlations resemble those given by these expressions. Note that $\mathcal{C}_2 \ll \mathcal{C}_1$. Deviations from this behavior are due to interference with the P waves. In the data at $p_{\rm lab} = 1546.2$ MeV/c it is still possible to recognize the shapes given above. Explicit expressions due to other transitions can be calculated, but in case of the spin correlations we do not learn much new. What is clear, however, is that we need the tensor-force transitions ${}^3D_1 \to {}^3S_1$ and ${}^3F_2 \to {}^3P_2$ to obtain the proper shape of the spin correlations.

Turning to the polarization and including only transitions with S- and P-wave final states, we have that

$$
P_y(\theta) = \mathrm{Im}(\mathcal{P}_1 \sin\theta + \mathcal{P}_2 \sin 2\theta) \quad .
$$

In this expression $\mathcal{P}_1$ comes from the interference of the ${}^3S_1$ and ${}^3D_1 \to {}^3S_1$ transitions with the ${}^3P_1$, ${}^3P_2$, and ${}^3F_2 \to {}^3P_2$ transitions, whereas $\mathcal{P}_2$ is the result of the mutual interference of the P waves only. Thus we understand the $\sin\theta$ shape very close to threshold and the $\sin 2\theta$ shape that becomes more important at higher energies. Again it seems unlikely that the proper shape of the polarization at all energies can be obtained without tensor-force transitions, since the ${}^3F_2 \to {}^3P_2$ transition makes a substantial contribution. The same is true for the interference of the ${}^3D_1 \to {}^3S_1$ transition with the P-wave transitions.

C. Partial-wave analysis of the reaction $\overline{p}p \to \overline{\Lambda}\Lambda$

In the previous sections we have presented the results of a coupled-channels model that gives a very good description of the available data on $\overline{p}p \to \overline{\Lambda}\Lambda$. In our opinion the good results are mainly due to the use of a coupled-channels formalism, to the quality of the intermediate- and long-range interaction, and to the phenomenological treatment of the very complicated short-range dynamics. In this section we want to look at the results from a different angle, namely, we will argue that what we in fact can do is perform a partial-wave analysis (PWA) of the reaction $\overline{p}p \to \overline{\Lambda}\Lambda$ close to threshold. We mentioned in the introduction that the method of calculation used is essentially the same as the one used in the Nijmegen phase-shift or partial-wave analyses (PWA) of all low-energy pp scattering data below $T_{\rm lab}$ = 350 MeV [25, 26]. Let us look at the pp case for a moment in order to compare it to our analysis of the reaction $\overline{p}p \to \overline{\Lambda}\Lambda$.

In a PWA one attempts to achieve a model-independent parametrization of the partial waves as a function of energy. A well-known model-independent way to describe low-energy scattering data is for example the effective-range formalism. One has to realize, however, that even in the relatively simple case of single-channel pp scattering, it is necessary to supply a substantial amount of theoretical input in order to obtain good results. In a pp PWA one has to take into account the correct electromagnetic interaction, including relativistic corrections like the vacuum polarization and the magnetic-moments interaction, and the one-pion-exchange potential. These theoretically well-known interactions can be considered as model-independent. The description is improved by using as intermediate-range interaction a realistic heavy-boson-exchange potential. In the formalism used in [25, 26] the theoretically well-founded long-range interaction and the semi-phenomenological intermediate-range interaction are used in the Schrödinger equation and the short-range interaction is parametrized via the energy-dependent P matrix. The P-matrix parameters are fitted to the data. With this method very good results are obtained. As a consequence, one now has a good idea about the behavior of the model-independent phase shifts.

A PWA of the low-energy np scattering data below $T_{\rm lab} = 350$ MeV poses already much more problems. Here one has both isospin $I = 0$ and $I = 1$. Since it is impossible to determine all amplitudes from the data, the $I = 1$ amplitudes are taken over from the pp case, after applying corrections for electromagnetic effects and mass differences. So in the np case even more theoretical input than in the pp case is required to obtain good results.

The same techniques are used in our analysis of the reaction $\overline{p}p \to \overline{\Lambda}\Lambda$. The generalization to the case of multichannel antibaryon-baryon scattering is straightforward. Although the method of analysis is probably as model-independent as one can hope to achieve at this stage, one cannot expect the results to be as unique as those of a pp PWA. The complexity of the problem necessitates the use of a lot of theoretical input. The long-range interaction, the Coulomb force, the one-pion-exchange, and the one-kaon-exchange interaction, are model-independent. For the intermediate-range a semi-phenomenological meson-exchange potential is used. Here the validity of SU(3) symmetry for the meson-baryon coupling constants is assumed. As in the pp case, the use of heavy-boson-exchanges, like K^* exchange in $\overline{p}p \to \overline{\Lambda}\Lambda$, improves the description of the data. The short-range interaction, which in the case of antibaryon-baryon scattering is particularly complicated, is parametrized.

In order to avoid systematic errors, we do not include the spin-correlation data now, for

the reasons mentioned in the previous subsection. The data-set used in the PWA includes the cross sections and the polarizations, a total of 142 observables at six different energies. We now reach an excellent $\chi^2_{\rm min} = 147.7$.

As results of the partial-wave analysis we give in Table IX the 'model-independent' S-matrix elements for the relevant $\overline{p}p \to \overline{\Lambda}\Lambda$ transitions as they follow from the fit to the data. In view of the quality of the fit, one can be confident that the important transitions are well described. It is not possible, however, to determine the behavior of all partial waves. For instance, the singlet transitions are not visible at all in the data. But even in most of these cases one expects that the tail of the strangeness-exchange potential, which is more-or-less model-independent, determines to a large extent the dynamics.

In tabulating the S-matrix elements we extract the kinematical effects due to the vicinity of the threshold by writing the elements in the following way

$$S \;=\; p_f^{\ell_f+\frac{1}{2}} \mathcal{S} p_i^{\ell_i+\frac{1}{2}} \quad . \tag{30}$$

Here p_i and p_f are the center-of-mass momenta in the initial and final state. The complex numbers $\mathcal{S}$ are written in the form $\mathcal{S} = |\mathcal{S}| \exp i\Phi$. For each transition the absolute values $|\mathcal{S}|$ and the phases Φ are given in Table IX. As can be seen from Table IX this representation of the S-matrix elements is quite nice, since many of the phases Φ are remarkably constant in the energy region under consideration.

In the pp PWA the method of analysis allowed a determinination of the neutral-pion coupling constant from the data [26]. We realized that analogously it should be possible to extract the ΛpK coupling constant from the data on $\overline{p}p \to \overline{\Lambda}\Lambda$. The coupling constant, which appears in the tail of the one-kaon-exchange potential used outside $r = b$, is added as a further parameter and included in the parameter set that is fitted to the data. We found [43] that the result was consistent with the prediction from SU(3) symmetry, if one assumes the pseudovector type of interaction (see Table II). Details can be found in Ref. [43]. We stress that the reliability of the result depends crucially on the type of PWA we present here, which is as model-independent as possible.

D. Outlook

So far our model could only be applied to the data on $\overline{p}p \to \overline{p}p$ and $\overline{p}p \to \overline{\Lambda}\Lambda$. However, from the experimental side there is more in store for the future. The reaction $\overline{p}p \to \overline{\Lambda}\Sigma^0, \overline{\Sigma^0}\Lambda$ is being studied [6]. Very recently, more data on $\overline{p}p \to \overline{\Lambda}\Lambda$ at higher energies have become available [44]. Especially interesting are the prospects of obtaining data on the Σ production reactions and in particular on the double-charge-exchange strangeness-exchange reaction $\overline{p}p \to \overline{\Sigma^-}\Sigma^-$, which can possibly provide a window on physics beyond the OBE picture. A simultaneous analysis of all these data on antihyperon-hyperon production is of course a difficult enterprise, but the model presented here is well suited to do this job. In the way demonstrated here for the case of the reaction $\overline{p}p \to \overline{\Lambda}\Lambda$, the model can be used to perform partial-wave analyses of all the reactions $\overline{p}p \to \overline{Y}Y$ close to threshold. In this way a lot of information can be obtained on the dynamics of strangeness production in antiproton-proton scattering. We have shown how the data on $\overline{p}p \to \overline{\Lambda}\Lambda$ clearly reflect the presence of a strong tensor force due to the combined exchange of the $K(494)$ and $K^*(892)$ mesons.

With data on several reactions available, parameters can be constrained from SU(2) or SU(3) symmetry in order to limit their number. One hopes especially to reduce as much as possible the number of final-state parameters. One major goal of this work will be to obtain more information on the coupling of the strange mesons $K(494)$ and $K^*(892)$ to baryons. We intend to extract both coupling constants $f_{\Lambda pK}$ and $f_{\Sigma pK}$ from future data in the manner demonstated in Ref. [43] for the available data on $\overline{p}p \rightarrow \overline{\Lambda}\Lambda$. We hope to improve on the accuracy already obtained in [43]. This will be a more severe test for the validity of SU(3) symmetry and an independent determination of the $\alpha = F/(F+D)$ ratio.

ACKNOWLEDGMENTS

We would like to express our gratitude to dr. P. Timmers for his pioneering work on the reaction $\overline{p}p \rightarrow \overline{\Lambda}\Lambda$ from which we have benefited much. It is a pleasure to thank all the members of the PS185 collaboration at CERN for their interest in our work. In particular we are grateful to prof. dr. K. Kilian, dr. W. Dutty, dr. R. von Frankenberg, and dr. G. Sehl for sending us the experimental data on $\overline{p}p \rightarrow \overline{\Lambda}\Lambda$. R.T. would like to thank dr. S. Ohlsson of the PS185 group for several stimulating discussions. Part of this work was included in the research program of the Stichting voor Fundamenteel Onderzoek der Materie (F.O.M.) with financial support from the Nederlandse Organisatie voor Wetenschappelijk Onderzoek (N.W.O.).

APPENDIX A: FLAVOR SU(3) FORMALISM

An irreducible representation of the flavor group SU(3), denoted by $\{\mu\}$, has a matrix representation in a complex vector space of dimension N_μ spanned by the basis $\xi_\nu^{(\mu)}$, where ν summarizes the SU(3) magnetic quantum numbers, $\nu = (I, Y, m)$, with m the z-component of the isospin. Note that $-\nu \equiv (I, -Y, -m)$. For an element $U(\alpha)$ of the group we have

$$U(\alpha)\xi_\nu^{(\mu)} = \xi_{\nu'}^{(\mu)} D_{\nu'\nu}^{(\mu)}(\alpha) \quad . \tag{A1}$$

This defines the matrix representation $D^{(\mu)}(\alpha)$ of the irrep $\{\mu\}$. The contragredient representation $\{\mu^*\}$, in general not equivalent to $\{\mu\}$, is defined by the basis

$$\xi_\nu^{(\mu^*)} = (-)^{Q(\nu)} \xi_{-\nu}^{(\mu)*} \quad , \tag{A2}$$

in a manner consistent with the Condon-Shortley phase convention [30]. The matrix representation of the contragredient representation $\{\mu^*\}$ is related to that of $\{\mu\}$ by

$$D^{(\mu^*)}(\alpha) = (-)^{Q(-\nu')} D^{(\mu)*}_{-\nu'-\nu}(\alpha)(-)^{Q(\nu)} \quad . \tag{A3}$$

Using these conventions we can now construct one-particle states for mesons, baryons, and antibaryons in a Fock space by the action of the usual creation and annihilation operators on the vacuum, keeping in mind that mesons are assigned to selfconjugate representations $\{\mu^*\}$=$\{\mu\}$

$$\begin{aligned} |\mathbf{k}, \mu, \nu\rangle &= a_\nu^{(\mu)\dagger}(\mathbf{k})|0\rangle \quad , \\ |\mathbf{p}, s, \mu, \nu\rangle &= b_\nu^{(\mu)\dagger}(\mathbf{p}, s)|0\rangle \quad , \\ |\mathbf{p}, s, \mu^*, \nu\rangle &= d_\nu^{(\mu^*)\dagger}(\mathbf{p}, s)|0\rangle \quad . \end{aligned} \tag{A4}$$

Here s symbolizes the z-component of the spin. In the expression for the meson state possible spin indices are suppressed. These annihilation operators thus transform with $D^{(\mu)}$ ($D^{(\mu^*)}$ for the antibaryon) whereas the corresponding creation operators transform with $D^{(\mu)*}$ ($D^{(\mu^*)*}$ for the antibaryon). The canonical (anti)commutation relations, from which follow the normalizations of the one particle states, are given by

$$\begin{aligned} \left[a_{\nu'}^{(\mu')}(\mathbf{k}'), a_\nu^{(\mu)\dagger}(\mathbf{k})\right] &= (2\pi)^3\ 2E_k\ \delta^{(3)}(\mathbf{k}-\mathbf{k}')\delta_{\mu\mu'}\delta_{\nu\nu'} \quad , \\ \left\{b_{\nu'}^{(\mu')}(\mathbf{p}', s'), b_\nu^{(\mu)\dagger}(\mathbf{p}, s)\right\} &= (2\pi)^3\ 2E_p\ \delta^{(3)}(\mathbf{p}-\mathbf{p}')\delta_{\mu\mu'}\delta_{\nu\nu'}\delta_{ss'} \quad , \\ \left\{d_{\nu'}^{(\mu')}(\mathbf{p}', s'), d_\nu^{(\mu)\dagger}(\mathbf{p}, s)\right\} &= (2\pi)^3\ 2E_p\ \delta^{(3)}(\mathbf{p}-\mathbf{p}')\delta_{\mu\mu'}\delta_{\nu\nu'}\delta_{ss'} \quad , \end{aligned} \tag{A5}$$

where $E_p = \sqrt{\mathbf{p}^2 + m^2}$. Finally second-quantized meson and baryon fields are defined by

$$\phi_\nu^{(\mu)}(x) = \int \frac{d^3\mathbf{k}}{(2\pi)^3 2E_k} \left(a_\nu^{(\mu)}(\mathbf{k})e^{ikx} + (-)^{Q(\nu)} a_{-\nu}^{(\mu)\dagger}(\mathbf{k})e^{-ikx}\right) \quad , \tag{A6}$$

$$\psi_\nu^{(\mu)}(x) = \int \frac{d^3\mathbf{p}}{(2\pi)^3 2E_p} \sum_s \left(b_\nu^{(\mu)}(\mathbf{p}, s)u(\mathbf{p}, s)e^{ipx} + (-)^{Q(\nu)} d_{-\nu}^{(\mu^*)\dagger}(\mathbf{p}, s)v(\mathbf{p}, s)e^{-ipx}\right) \quad . \tag{A7}$$

The space-time signature used is $(-+++)$. Possible spin indices of the meson field are again suppressed. The fields defined here transform with $D^{(\mu)*}$, whereas the Dirac conjugate field, given by

$$\overline{\psi}^{(\mu)}_{\nu}(x) = \psi^{(\mu)\dagger}_{\nu}(x)\gamma_4 \quad , \tag{A8}$$

transforms with $D^{(\mu)}$.

APPENDIX B: PARTIAL-WAVE DECOMPOSITION OF THE OBSERVABLES

Consider a scattering proces of two spin 1/2 particles where the beam comes in along the z-axis and the y-axis lies normal to the scattering plane. On the spin singlet-triplet basis and in the absence of spin-changing transitions, the scattering amplitude can be written as

$$\begin{aligned} M_{m'm}(\theta,\phi) = \sum_{J,\ell,\ell'} \sqrt{4\pi(2\ell+1)}\; i^{\ell-\ell'}\; C\begin{pmatrix} \ell' & & s & J \\ m-m' & & m' & m \end{pmatrix} C\begin{pmatrix} \ell & s & J \\ 0 & m & m \end{pmatrix} \\ Y^{(\ell')}_{m-m'}(\theta,\phi)\; \langle f;\ell' s|(S^J-1)|i;\ell s\rangle/2ik \quad . \end{aligned} \tag{B1}$$

For singlet states this expression reduces to

$$M_{SS}(\theta) \;=\; \sum_{\ell} \sqrt{4\pi(2\ell+1)}\; Y^{(\ell)}_0(\theta)\; \langle f;\ell s|(S^\ell-1)|i;\ell s\rangle/2ik \quad . \tag{B2}$$

The dependence on θ is determined by the orbital angular momentum of the final state. It can be shown from rotational invariance that the following symmetry relation holds

$$M_{m'm}(\theta,0) \;=\; (-)^{m'-m}\; M_{-m'-m}(\theta,0) \quad , \tag{B3}$$

which leaves us with five independent amplitudes. In terms of these amplitudes $M_{m'm}$ the observables defined in section 2 read

$$\begin{aligned} I_0 &= \tfrac{1}{2}\,\{|M_{11}|^2+|M_{10}|^2+|M_{1-1}|^2+|M_{01}|^2+\tfrac{1}{2}|M_{00}|^2+\tfrac{1}{2}|M_{SS}|^2\} \\ I_0P_y &= -\tfrac{1}{2}\sqrt{2}\;\mathrm{Im}\,\{(M_{11}-M_{1-1})M^*_{01}+M_{10}M^*_{00}\} \\ I_0C_{xx} &= \tfrac{1}{4}\,\{-|M_{SS}|^2+|M_{00}|^2+2|M_{01}|^2-2|M_{10}|^2+4\mathrm{Re}(M_{1-1}M^*_{11})\} \\ I_0C_{yy} &= \tfrac{1}{4}\,\{-|M_{SS}|^2+|M_{00}|^2+2|M_{01}|^2+2|M_{10}|^2-4\mathrm{Re}(M_{1-1}M^*_{11})\} \\ I_0C_{zz} &= \tfrac{1}{4}\,\{-|M_{SS}|^2-|M_{00}|^2-2|M_{01}|^2+2|M_{10}|^2+2|M_{11}|^2+2|M_{1-1}|^2\} \\ I_0C_{xz} &= \tfrac{1}{2}\sqrt{2}\;\mathrm{Re}\,\{(M_{11}-M_{1-1})M^*_{01}+M_{10}M^*_{00}\} \\ I_0S &= \tfrac{1}{4}|M_{SS}|^2 \quad . \end{aligned} \tag{B4}$$

The different terms occurring in $M_{m'm}(\theta,0)$ apart from the factors $(S^J-1)/2ik$ are collected in Table X.

In order to conform to the convention of the experimentalists to use two sets of body-fixed axes for the final-state particles, a rotation has to be performed in the x-z scattering plane, and C_{xx}, C_{xz}, and C_{zz} change sign. Substituting the results of Table X in the expression for the scattering amplitude provides us with a useful partial-wave decomposition of the observables.

REFERENCES

[1] P.D. Barnes *et al.*, Phys. Lett. B **189** (1987) 249.
[2] P.D. Barnes *et al.*, Phys. Lett. B **199** (1987) 147.
[3] P.D. Barnes *et al.*, Phys. Lett. B **229** (1989) 432.
[4] J. Button *et al.*, Phys. Rev. **121** (1961) 1788;
X. Xuong *et al.*, Phys. Rev. **128** (1962) 1849;
J. Badier *et al.*, Phys. Lett. **25B** (1967) 152;
B.Y. Oh *et al.*, Nucl. Phys. **B51** (1973) 57;
H.W. Atherton *et al.*, Nucl. Phys. **B69** (1974) 1;
N. Kwak *et al.*, Nuovo Cimento **23A** (1974) 610;
H. Becker *et al.*, Nucl. Phys. **B141** (1978) 48;
S.M. Jacobs *et al.*, Phys. Rev. D **17** (1978) 1187.
[5] B. Jayet *et al.*, Nuovo Cimento **45A** (1978) 371.
[6] S. Ohlsson, thesis University of Uppsala, (1990);
P.D. Barnes *et al.*, Phys. Lett. B **246** (1990) 273.
[7] P.H.A. Timmers, thesis University of Nijmegen, (1985).
[8] D.P. Roy, Phys. Rev. **146** (1966) 1218.
[9] G. Plaut, Nucl. Phys. **B35** (1971) 221.
[10] F. Tabakin and R.A. Eisenstein, Phys. Rev. C **31** (1985) 1857.
[11] P.H. Timmers, W.A. van der Sanden, and J.J. de Swart,
Phys. Rev. D **29** (1984) 1928.
[12] J.A. Niskanen, Helsinki preprint HU-TFT-85-28 (1985).
[13] M. Kohno and W. Weise, Phys. Lett. B **179** (1986) 15;
Phys. Lett. B **206** (1988) 584.
[14] T. Hippchen, B. Holzenkamp, K. Holinde, and J. Speth,
in "Physics at LEAR with Low-Energy Antiprotons",
ed. C. Amsler *et al.* (Harwood, New York, 1988), p.371.
[15] P. Lafrance, B. Loiseau, and R. Vinh Mau,
Phys. Lett. B **214** (1988) 317;
P. Lafrance and B. Loiseau, Nucl. Phys. **A528** (1991) 557.
[16] R.G.E. Timmermans, Th.A. Rijken, and J.J. de Swart,
Proceedings of the International Symposium on
Strangeness in Hadronic Matter, Bad Honnef (1987),
Nucl. Phys. **A479** (1988) 383c.
[17] R.G.E. Timmermans, T.A. Rijken, and J.J. de Swart,
in "Physics at LEAR with Low-Energy Antiprotons",
ed. C. Amsler *et al.* (Harwood, New York, 1988), p.357.
[18] J.J. de Swart, R. Timmermans, and T.A. Rijken,
Proceedings of the Third Conference on Intersections Between
Particle and Nuclear Physics, Rockport Maine (1988), p.366;
J.J. de Swart, T.A. Rijken, P.M. Maessen, and R.G.E. Timmermans,
Proceedings of the 1988 International Symposium on
Hypernuclear and Low-Energy Kaon Physics, Padova (1988),
Nuovo Cimento **102A** (1989) 203.

[19] M.M. Nagels, T.A. Rijken, and J.J. de Swart,
Phys. Rev. D **17** (1978) 768.
[20] P.M.M. Maessen, Th.A. Rijken, and J.J. de Swart,
Phys. Rev. C **40** (1989) 2226.
[21] S. Furui and A. Faessler, Nucl. Phys. **A468** (1987) 669.
[22] H.R. Rubinstein and H. Snellman, Phys. Lett. **165B** (1985) 187.
[23] P. Kroll and W. Schweiger, Nucl. Phys. **A474** (1987) 608.
[24] R.L. Jaffe and F.E. Low, Phys. Rev. D **19** (1979) 2105.
[25] J.R. Bergervoet, P.C. van Campen, W.A. van der Sanden,
and J.J. de Swart, Phys. Rev. C **38** (1988) 15.
[26] J.R. Bergervoet, P.C. van Campen, R.A.M. Klomp, J.-L. de Kok,
T.A. Rijken, V.G.J. Stoks, and J.J. de Swart,
Phys. Rev. C **41** (1990) 1435.
[27] L. Durand III and J. Sandweiss, Phys. Rev. **135** (1964) B540.
[28] M.H. Partovi and E.L. Lomon, Phys. Rev. D **2** (1970) 1999;
K. Erkelenz, Phys. Rep. **13C** (1974) 191;
J.J. de Swart and M.M. Nagels, Fortschr. Phys. **26** (1978) 215.
[29] A.A. Logunov and A.N. Tavkhelidze, Nuovo Cimento **29** (1963) 380;
R. Blankenbecler and R. Sugar, Phys. Rev. **142** (1966) 1051;
V.G. Kadyshevsky, Nucl. Phys. **B6** (1968) 125;
V.G. Kadyshevsky and M.D. Mateev, Nuovo Cimento **55** (1968) 275.
[30] J.J. de Swart, Rev. Mod. Phys. **35** (1963) 916.
[31] F.E. Low, Phys. Rev. D **12** (1975) 163;
S. Nussinov, Phys. Rev. Lett. **34** (1975) 1286.
[32] A.M. Green, Nucl. Phys. **33** (1963) 218.
[33] R.H. Dalitz and F. von Hippel, Phys. Lett. **10** (1964) 153.
[34] J.J. de Swart, M.M. Nagels, T.A. Rijken, and P.A. Verhoeven,
Springer Tracts in Mod. Phys. **60** (1971) 138.
[35] H.W. Atherton *et al.*, Phys. Lett. **42B** (1972) 522.
[36] E. Eisenhandler *et al.*, Nucl. Phys. **B113** (1976) 1.
[37] R.A. Kunne *et al.*, Phys. Lett. B **206** (1988) 557.
[38] R. Kunne, thesis University of Amsterdam, (1988);
R.A. Kunne *et al.*, Nucl. Phys. **B323** (1989) 1.
[39] R. von Frankenberg, thesis University of Erlangen-Nürnberg, (1987).
[40] W. Dutty, thesis University of Freiburg, (1988).
[41] O.D. Dalkarov, K.V. Protasov, and I.S. Shapiro, "P-wave
enhancement in baryon-antibaryon systems at low energy",
Preprint 37, Moscow, FIAN, 1988;
Int. Jour. of Mod. Phys. A **5** (1990) 2155.
[42] M.M. Nagels and T.A. Rijken, University of Nijmegen,
internal report THEP 70-11 (1970).
[43] R.G.E. Timmermans, Th.A. Rijken, and J.J. de Swart,
Phys. Lett. B **257** (1991) 227.
[44] P.D. Barnes *et al.*, Nucl. Phys. **A526** (1991) 575.

TABLES

	$E_{\rm t}$ (MeV)	$p_{\rm lab}$ (MeV/c)	I	ΔQ	ΔS
$\overline{p}p$	1877	0	0,1	0	0
$\overline{n}n$	1879	100	0,1	1	0
$\overline{\Lambda}\Lambda$	2231	1435	0	1	1
$\overline{\Lambda}\Sigma^0$,$\overline{\Sigma^0}\Lambda$	2308	1653	1	1	1
$\overline{\Sigma^+}\Sigma^+$	2379	1853	0,1,2	0	1
$\overline{\Sigma^0}\Sigma^0$	2385	1871	0,2	1	1
$\overline{\Sigma^-}\Sigma^-$	2395	1899	0,1,2	2	1
$\overline{\Xi^0}\Xi^0$	2630	2582	0,1	1	2
$\overline{\Xi^-}\Xi^-$	2643	2620	0,1	2	2

TABLE I. Antibaryon-baryon final states accessible at LEAR with their threshold energies in $\overline{p}p$ scattering. I denotes the isospin. ΔQ and ΔS refer to the number of charge and strangeness quanta exchanged.

multiplet	J^{PC}	$-\mathcal{L}_{int}$
scalar	0^{++}	$g\overline{\psi}\psi\phi_S$
pseudoscalar	0^{-+}	$i\frac{f}{m}\overline{\psi}\gamma_\mu\gamma_5\psi\partial^\mu\phi_P$; $ig\overline{\psi}\gamma_5\psi\phi_P$
vector	1^{--}	$ig\overline{\psi}\gamma_\mu\psi\phi_V^\mu + \frac{f}{4M}\overline{\psi}\sigma_{\mu\nu}\psi(\partial^\mu\phi_V^\nu - \partial^\nu\phi_V^\mu)$
tensor	2^{++}	$\left[\frac{g}{2M}\overline{\psi}(\gamma_\mu\partial_\nu + \gamma_\nu\partial_\mu)\psi - \frac{f}{4M^2}\partial_\mu\overline{\psi}\partial_\nu\psi\right]\phi_T^{\mu\nu}$

TABLE II. Interactions $-\mathcal{L}_{int}$ of baryons and mesons. m and M are scaling masses, chosen as the mass of the charged pion and proton respectively. For pseudoscalars both pseudovector and pseudoscalar couplings are shown.

• vertex factor:		$\sum_\gamma g_{12}(\gamma) \begin{pmatrix} \mu_1 & \mu & \mu_{2_\gamma} \\ \nu_1 & \nu & \nu_2 \end{pmatrix} \Gamma$
– with $(-)^{Q(\nu_1)} + (-)^{Q(\nu_2)} + (-)^{Q(\nu)} = 1$		from charge conservation
• internal lines:		
– meson propagator:		$\delta_{\mu\mu'}\delta_{\nu-\nu'}(-)^{Q(\nu)}D_F(k)$
– baryon propagator:		$\delta_{\mu\mu'}\delta_{\nu\nu'}S_F(p)$
• external lines:		
– absorbed baryon:		$u(\mathbf{p}, s)$
– absorbed antibaryon:		$\overline{v}(\mathbf{p}, s)(-)^{Q(\nu)}$
– emitted baryon:		$\overline{u}(\mathbf{p}, s)$
– emitted antibaryon:		$v(\mathbf{p}, s)(-)^{Q(\nu)}$
• permutation factor: (from normal ordering)	for $\overline{B}_1 B_2 \to \overline{B}_3 B_4$	$\delta_P = -1$

TABLE III. Feynman rules for $-iM_{fi}$ for baryons and mesons with unbroken flavor SU(3) symmetry. The corresponding Lagrangian is given in equation 21.

$I=0, Y=0$	$\overline{N}N$	$\overline{\Lambda}\Lambda$	$\overline{\Sigma}\Sigma$
$\overline{N}N$	$3g^2_{NN\pi}$; $g^2_{NN\eta}$	-$\sqrt{2}g^2_{\Lambda NK}$	$\sqrt{6}g^2_{\Sigma NK}$
$\overline{\Lambda}\Lambda$	-$\sqrt{2}g^2_{\Lambda NK}$	$g^2_{\Lambda\Lambda\eta}$	-$\sqrt{3}g^2_{\Lambda\Sigma\pi}$
$\overline{\Sigma}\Sigma$	$\sqrt{6}g^2_{\Sigma NK}$	-$\sqrt{3}g^2_{\Lambda\Sigma\pi}$	$2g^2_{\Sigma\Sigma\pi}$; $g^2_{\Sigma\Sigma\eta}$
$I=1, Y=0$	$\overline{N}N$	$(\overline{\Lambda}\Sigma+\overline{\Sigma}\Lambda)/\sqrt{2}$	$\overline{\Sigma}\Sigma$
$\overline{N}N$	-$g^2_{NN\pi}$; $g^2_{NN\eta}$	-$\sqrt{2}g_{\Lambda NK}g_{\Sigma NK}$	$2g^2_{\Sigma NK}$
$(\overline{\Lambda}\Sigma+\overline{\Sigma}\Lambda)/\sqrt{2}$	-$\sqrt{2}g_{\Lambda NK}g_{\Sigma NK}$	$g^2_{\Lambda\Sigma\pi}$; $g_{\Lambda\Lambda\eta}g_{\Sigma\Sigma\eta}$	$\sqrt{2}g_{\Lambda\Sigma\pi}g_{\Sigma\Sigma\pi}$
$\overline{\Sigma}\Sigma$	$2g^2_{\Sigma NK}$	$\sqrt{2}g_{\Lambda\Sigma\pi}g_{\Sigma\Sigma\pi}$	$g^2_{\Sigma\Sigma\pi}$; $g^2_{\Sigma\Sigma\eta}$

TABLE IV. Symmetry factors $G(IY; I''Y'')$ for pseudoscalar octet exchange.

M		ΛNM	ΣNM
$K(494)$	f	-0.27045	0.07904
	g	(-3.98122)	(1.20749)
$K^*(892)$	g	-1.54408	-0.89147
	f	-3.36708	1.69315
$K_0^*(1000)$	g	-2.63359	-2.00682
$K_2^*(1430)$	g	-0.81469	-0.51408

TABLE V. Coupling constants of the strange mesons. For $K(494)$ exchange also the equivalent pseudoscalar coupling constants are given in parentheses for comparison.

$\overline{\Lambda}\Lambda\to\overline{\Lambda}\Lambda$	$V(r<b)$	$\overline{p}p\to\overline{\Lambda}\Lambda$	θ (degrees)
$^3S_1$	94 ± 26	$^3S_1,^3D_1\to^3S_1$	$-6.6^\circ\pm1.3^\circ$
$^3P_2$	422 ± 134	$^3P_{0,1,2}$	$4.9^\circ\pm1.1^\circ$
rest	-121 ± 23	$^3D_3$	$8.6^\circ\pm1.7^\circ$
		$^3F_2\to^3P_2$	$-1.7^\circ\pm1.2^\circ$
		$^3G_3\to^3D_3$	$2.9^\circ\pm1.9^\circ$

TABLE VI. Parameter set of our fit. The $\overline{p}p\to\overline{p}p$ initial-state annihilation parameter is $W=-617\pm81$ MeV, while for the $\overline{\Lambda}\Lambda\to\overline{\Lambda}\Lambda$ final state it is $W=-182\pm17$ MeV.

$p_{\rm lab}$ (MeV/c)	Ref.	No. type	Rejected	Pred.norm	$\chi^2_{\rm min}$	χ^2/data
1435.95	[3, 39]	10 $d\sigma$		0.9819	11.6	1.2
	[3, 39]	5 P_y	all	0.9984	11.3	2.3
1436.95	[3, 39]	10 $d\sigma$	$\cos\theta=0.3$	1.0267	9.3	1.0
	[3, 39]	5 P_y		1.0047	3.3	0.7
1445.35	[3, 39]	20 $d\sigma$		1.0166	21.9	1.1
	[3, 39]	10 P_y		0.9993	7.2	0.7
1476.5	[1]	20 $d\sigma$		0.8594	17.3	0.9
	[1]	5 P_y		0.9736	11.9	2.4
1507.5	[1]	20 $d\sigma$		0.9405	22.2	1.1
	[1]	5 P_y		1.0009	4.4	0.9
1546.2	[2, 40]	20 $d\sigma$		1.0765	23.9	1.2
	[2, 40]	14 P_y	$\cos\theta=0.55$	1.0124	11.1	0.9
	[2, 40]	5 C_{xx}		0.9829	9.6	1.9
	[2, 40]	5 C_{yy}		1.0235	5.5	1.1
	[2, 40]	5 C_{zz}		1.0266	12.3	2.5
	[2, 40]	5 C_{xz}		0.9941	9.1	1.8

TABLE VII. Reference Table for the PS185 LEAR data on $\overline{p}p\to\overline{\Lambda}\Lambda$.

$p_{\rm lab}$ (MeV/c)	1435.95	1436.95	1445.35	1476.5	1507.5	1546.2
ε (MeV)	0.24	0.59	3.5	14.5	25.5	39.1
$^3D_1 \to {}^3S_1$	0.89	1.36	2.9	4.2	4.3	4.0
$^3F_2 \to {}^3P_2$	0.01	0.05	0.7	4.0	6.7	8.9
$^3G_3 \to {}^3D_3$				1.2	4.0	9.6
$^1S_0$		0.01				
$^1P_1$					0.1	0.1
$^3S_1$	0.08	0.12	0.3	0.5	0.6	0.7
$^3P_0$		0.01	0.1	0.5	0.6	0.7
$^3P_1$	0.01	0.04	0.5	2.9	4.5	5.3
$^3P_2$	0.01	0.03	0.4	2.1	3.7	5.1
$^3D_1$				0.1	0.2	0.5
$^3D_2$				0.2	0.6	1.4
$^3D_3$				0.4	1.3	3.2
$^3F_3$					0.1	0.2
$^3S_1 \to {}^3D_1$				0.1	0.3	0.8
$^3P_2 \to {}^3F_2$						0.1
$J \geq 4$					0.2	0.9
singlet $s = 0$	0.00	0.01	0.0	0.1	0.1	0.1
triplet $s = 1$	1.00	1.60	4.9	16.1	27.3	41.3
total	1.00	1.61	4.9	16.2	27.3	41.4
experimental	0.84(20)	1.44(32)	4.86(42)	13.8(5)	26.6(7)	44.6(1.5)

TABLE VIII. Partial cross sections in μb for $\overline{p}p \to \overline{\Lambda}\Lambda$.

transition	$\overline{p}p \to \overline{\Lambda}\Lambda$	$^3S_1$		$^3D_1 \to {}^3S_1$		$^3S_1 \to {}^3D_1$		$^3D_1$		$^3P_0$		$^3P_2$		$^3F_2 \to {}^3P_2$	
$p_{\rm lab}$ (MeV/c)	ε (MeV)	$10^4\|\mathcal{S}\|$	Φ	$10^4\|\mathcal{S}\|$	Φ	$10^4\|\mathcal{S}\|$	Φ	$10^4\|\mathcal{S}\|$	Φ	$10^4\|\mathcal{S}\|$	Φ	$10^4\|\mathcal{S}\|$	Φ	$10^4\|\mathcal{S}\|$	Φ
1435.95	0.24	210	327	38.5	344	118	134	6.47	159	173	52	84.3	106	14.6	314
1436.95	0.59	202	325	37.2	342	117	134	6.39	160	172	53	83.8	106	14.5	314
1445.35	3.5	168	318	31.8	334	114	134	6.00	160	159	57	79.8	105	13.6	314
1476.5	14.5	103	308	22.6	317	107	134	5.05	159	110	63	67.0	102	11.0	312
1507.5	25.5	60.7	308	17.1	304	101	135	4.33	159	78.7	61	56.7	98	8.95	309
1546.2	39.1	30.8	343	12.2	290	92.4	137	3.56	159	56.1	54	46.7	92	7.06	304
transition	$\overline{p}p \to \overline{\Lambda}\Lambda$	$^3D_3$		$^3G_3 \to {}^3D_3$		$^3P_1$		$^3D_2$		$^1S_0$		$^1P_1$		$^1D_2$	
$p_{\rm lab}$ (MeV/c)	ε (MeV)	$10^4\|\mathcal{S}\|$	Φ	$10^4\|\mathcal{S}\|$	Φ	$10^4\|\mathcal{S}\|$	Φ	$10^4\|\mathcal{S}\|$	Φ	$10^4\|\mathcal{S}\|$	Φ	$10^4\|\mathcal{S}\|$	Φ	$10^4\|\mathcal{S}\|$	Φ
1435.95	0.24	33.5	146	2.23	303	183	184	6.84	259	52.6	177	18.6	255	4.38	302
1436.95	0.59	33.4	146	2.23	303	182	185	6.80	259	51.9	174	18.5	255	4.36	302
1445.35	3.5	32.9	146	2.15	304	170	189	6.52	259	49.3	160	17.3	257	4.23	302
1476.5	14.5	31.1	147	1.90	306	123	197	5.59	257	45.0	133	12.4	257	3.77	302
1507.5	25.5	29.3	149	1.67	309	89.6	197	4.79	256	42.7	115	9.11	250	3.35	302
1546.2	39.1	27.1	152	1.41	313	64.1	194	3.92	255	40.9	96	6.67	238	2.86	304

TABLE IX. S-matrix elements for the relevant transitions $\overline{p}p \to \overline{\Lambda}\Lambda$, with $\ell_f \leq 2$, parametrized according to equation 30, where p_i and p_f are given in units of MeV/$\hbar$c. The phase Φ is given in degrees.

$m'\ m$	0 0	0 1	1 -1	1 0	1 1
$^1S_0$	1	-	-	-	-
$^1P_1$	$3c$	-	-	-	-
$^3S_1$	1	0	0	0	1
$^3D_1 \to {}^3S_1$	$\sqrt{2}$	0	0	0	$-\frac{1}{2}\sqrt{2}$
$^3P_0$	c	0	0	$-\frac{1}{2}\sqrt{2}s$	0
$^3P_1$	0	$\frac{3}{4}\sqrt{2}s$	0	0	$\frac{3}{2}c$
$^3P_2$	$2c$	$-\frac{3}{4}\sqrt{2}s$	0	$\frac{1}{2}\sqrt{2}s$	$\frac{3}{2}c$
$^3F_2 \to {}^3P_2$	$\sqrt{6}c$	$\sqrt{\frac{21}{16}}s$	0	$\frac{1}{2}\sqrt{3}s$	$-\sqrt{\frac{21}{8}}c$

TABLE X. Terms occurring in $M_{m'm}$ apart from $(S-1)/2ik$. Here c and s stand for $\cos\theta$ and $\sin\theta$ respectively.

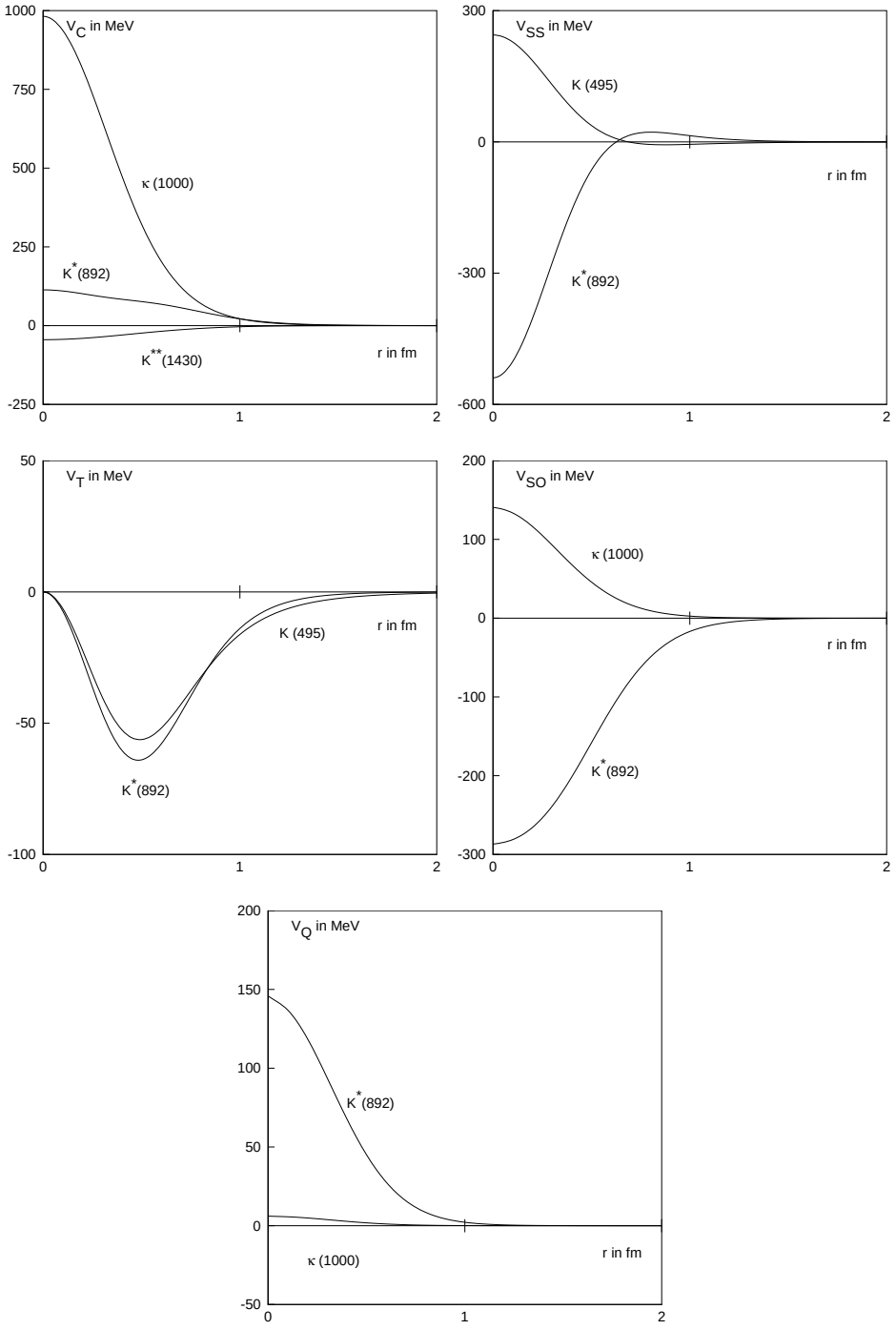

FIG. 1. Soft-core strangeness-exchange potentials for $\overline{p}p \rightarrow \overline{\Lambda}\Lambda$.

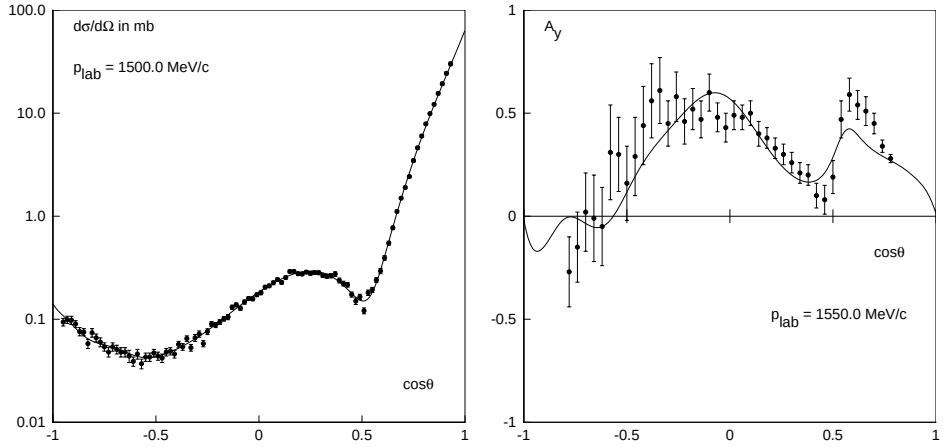

FIG. 2. Differential cross section in mb at momentum 1500 MeV/c and asymmetry at momentum 1550 MeV/c for $\overline{p}p \to \overline{p}p$.

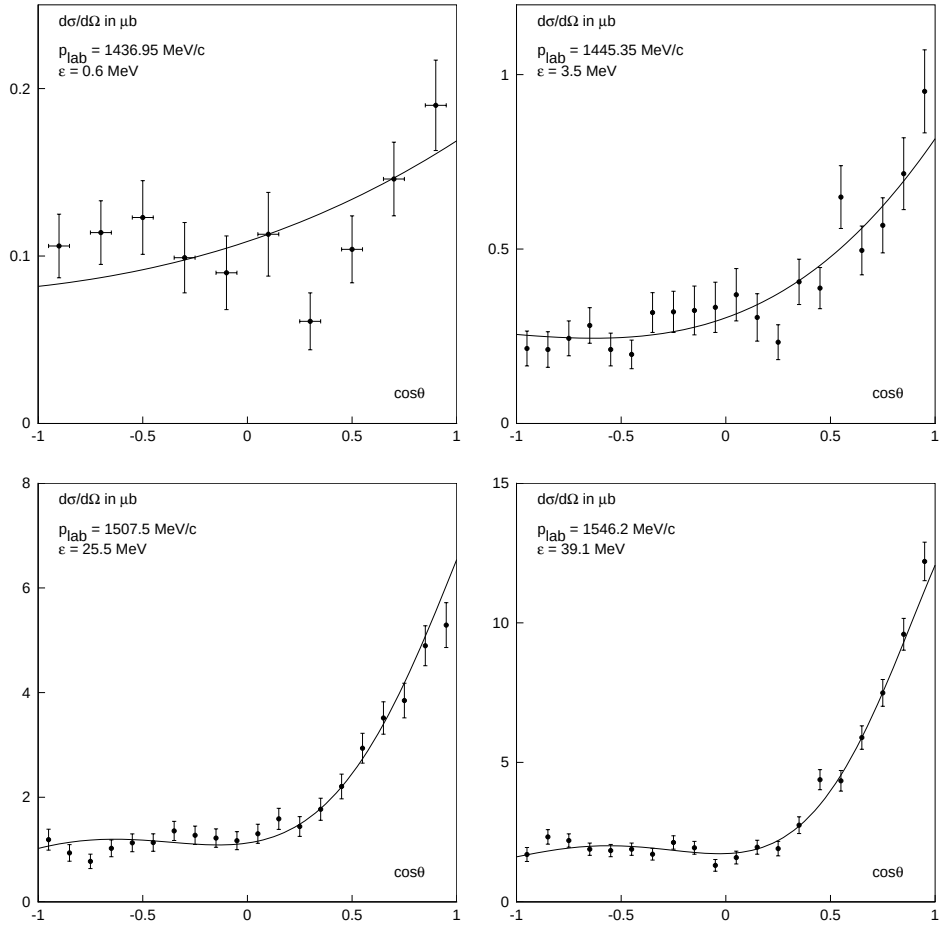

FIG. 3. Differential cross sections in μb at four energies for $\overline{p}p \to \overline{\Lambda}\Lambda$.

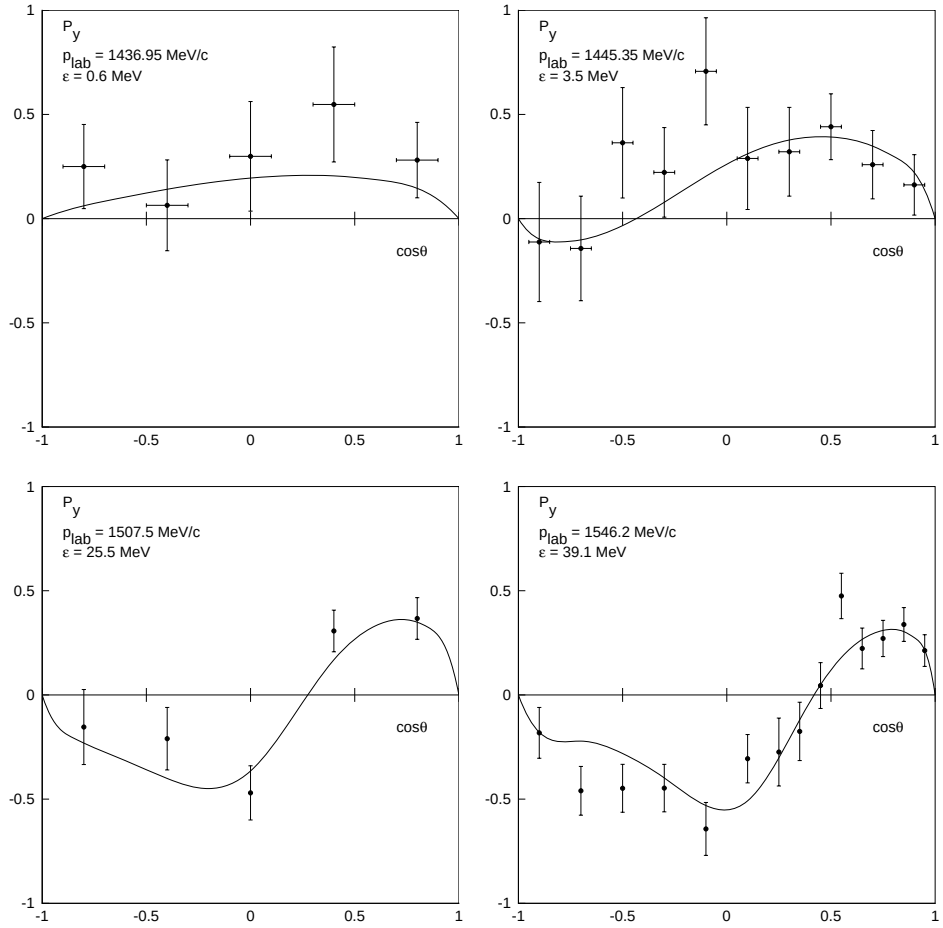

FIG. 4. Differential polarizations at four energies for $\overline{p}p \rightarrow \overline{\Lambda}\Lambda$.

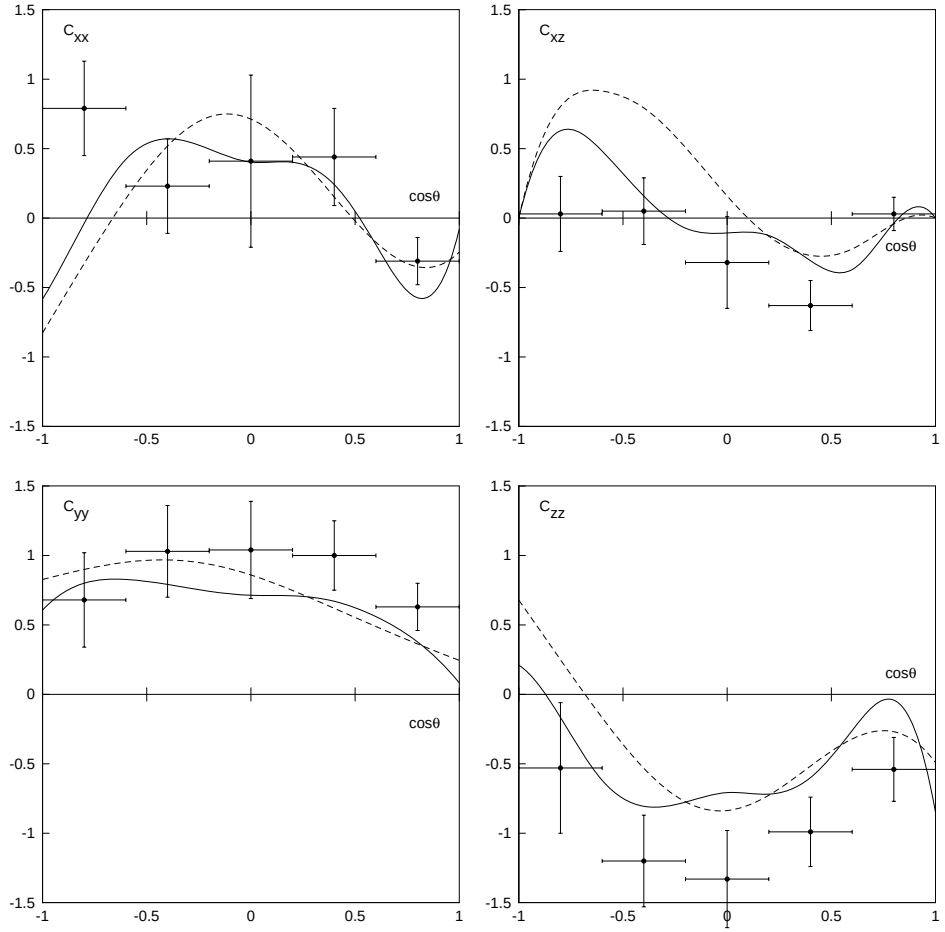

FIG. 5. Spin-correlation coefficients for $\overline{p}p \to \overline{\Lambda}\Lambda$ at momentum 1546.2 MeV/c. The dashed curve shows the spin correlations at 1445.35 MeV/c.

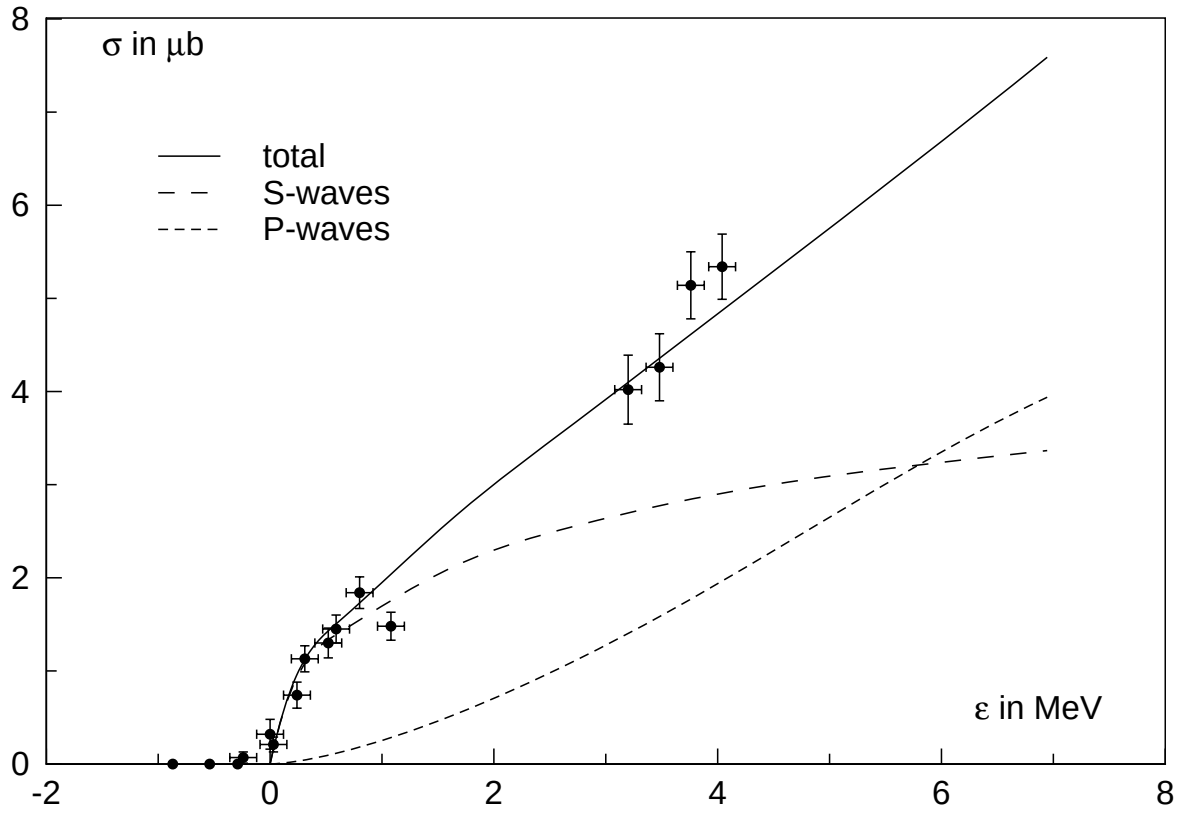

FIG. 6. S- and P-wave contributions to the cross section $\sigma_{\overline{\Lambda}\Lambda}$ in μb as a function of the excitation energy ε in MeV.